IEEE Access
Multidisciplinary | Rapid Review | Open Access Journal

Received July 16, 2019, accepted July 29, 2019, date of publication August 16, 2019, date of current version September 17, 2019.

Digital Object Identifier 10.1109/ACCESS.2019.2935751

Design of a New Seven-Dimensional Hyperchaotic Circuit and Its Application in Secure Communication

WENXIN YU[1,2,3], JING WANG[1], JUNNIAN WANG[3,4], HONGPING ZHU[1], MU LI[1], YAN LI[1], AND DAN JIANG[1,3]

[1]School of Information and Electrical Engineering, Hunan University of Science and Technology, Xiangtan 411201, China
[2]College of Electrical and Information Engineering, Hunan University, Changsha 410082, China
[3]Key Laboratory of Knowledge Processing Networked Manufacturing, Hunan University of Science and Technology, Xiangtan 411201, China
[4]School of Physics and Electronics, Hunan University of Science and Technology, Xiangtan 411201, China

Corresponding author: Jing Wang (1962949427@qq.com)

This work was supported in part by the China Postdoctoral Science Foundation under Project 2017M622574, in part by the Scientific Research Fund of Education Department of Hunan Province under Grant 17B094, in part by the Hunan University of Science and Technology Doctor Startup Fund under Grant E51892, and in part by the Hunan University of Science and Technology Student Research Innovation Program (SRIP) under Grant SZZ2019006.

ABSTRACT In the fields of physics, mathematics, communication, control, biology, etc., chaos is widely used, and it plays an important role in modern science and technology. In this paper, a new seven-dimensional hyperchaotic system is proposed and some related features of the hyperchaotic system are analyzed, including equilibrium stability, dissipation, bifurcation and Lyapunov exponent. The results show that the proposed hyperchaotic system exhibits hyperchaotic, chaotic, quasi-periodic and periodic dynamic behaviors. The seven-dimensional hyperchaotic system is implemented through experiments, and the phase diagrams of the circuit simulation are consistent with those of the numerical simulation, which verifies the physical realization of the hyperchaotic system. In view of chaos in some important fields, such as communication security and complex systems, the seven-dimensional hyperchaotic system is applied to signal encryption and decryption circuit design. Firstly, the proposed seven-dimensional hyperchaotic system is scaled and transformed into a hyperchaotic system that is easy to implement. Then an improved chaotic circuit module design is adopted. Finally, the seven-dimensional hyperchaotic circuit is designed to form a hyperchaotic secure communication circuit. The electronic circuit realizes the confidential communication and its experimental results prove the effectiveness of the designed scheme.

INDEX TERMS Seven-dimensional hyperchaotic, secure communication, circuit realization.

I. INTRODUCTION

Chaotic system refers to the existence of seemingly random irregular motion in a deterministic system. Its behavior is characterized by uncertainty, non-repeatable and unpredictable. This is chaotic phenomenon. Chaos is an intrinsic property of nonlinear dynamic systems and a ubiquitous phenomenon in nonlinear systems. Chaos theory is about the theory that a nonlinear system exhibits bifurcation under certain parameters, and the periodic motion and the aperiodic motion are entangled with each other, so that it leads to some aperiodic ordered motion. In 1963, when designing a three-dimensional model for atmospheric convection, Lorenz accidentally discovered the first chaotic system. Rössler discovered a three-dimensional chaotic system with more simple algebra than the Lorenz system in 1976. There are also many well-known three-dimensional chaotic systems, such as Arneodo system, Sprottsystems, Chen system, Lü-Chen system, Liu system, Cai system, T system, etc.. In recent years, with the wide application of chaos theory, people have conducted extensive research on chaos theory and achieved many new results [1]–[15].

In the study of secure communication using chaotic encryption, researchers have found that high-dimensional hyperchaotic systems are more difficult to interpret than low-dimensional chaotic systems [16]–[17]. The reasons are as follows: First, the chaotic signal band of a low-dimensional system is very narrow, so it is easy to lose the encryption

The associate editor coordinating the review of this article and approving it for publication was Cihun-Siyong Gong.

protection function when using a digital filter to separate the transmitted signal. Second, the chaotic dynamics of high-dimensional chaotic systems are more complex, and the frequency range of chaotic sequence signals is wider, so it is more difficult to be separated by filters when used for secure communication [18]–[21]. Chaotic sequence signals have very important application value for information encryption. Since Rossler proposed the concept of hyperchaos in 1979 [22], hyperchaos and basic systems have attracted much attention due to their irregularities and unpredictability. Reference [23] shows the basic questions about the Lyapunov exponent. To prove the actual sign of the Lyapunov exponent of the hyperchaotic system, three different algorithms are used to calculate the Laypunov exponent. In [24], a new hyperchaotic temperature fluctuation model is proposed, and the characteristics of the new hyperchaotic temperature fluctuation model are studied, such as phase portrait, static point, symmetry, invariance, Lyapunov characteristic exponent, and bifurcation analysis. In [25], two new practical and complex unbalanced hyperchaotic systems are designed firstly. Then, the synchronization method of the new system is designed by using the contraction theory. Finally, the proposed method is applied to verify the proposed method.

Hyperchaos has more complex features than chaos, including more unpredictability and higher order, more unusual attractors. Therefore, hyperchaotic signals can promote and enhance the security of chaos-based communication and digital audio encryption. For the above reasons, hyperchaos has become a research hotspot in the field of nonlinear control. At present, hyperchaotic research has been widely used in various aspects and has made significant progress.

In [26], Yang, *et al.* used return map-based methods to unmask some chaotic secure communication systems. In [27], Zheng, *et al.* proposed a digital chaotic secure communication by introducing a magnifying glass concept, which was used to enlarge and observe minor parameter mismatches to increase the sensitivity of the system. In [28], Álvarez, *et al.* described the security weakness of a recently proposed secure communication method based on parameter modulation of a chaotic system and an adaptive observer-based synchronization scheme. In [29], an implementation of a digital image encryption scheme based on a mixture of chaotic systems was reported. In [30], a system-oriented analysis of the encryption efficiency of chaotic communication systems consisting of lasers subject to all-optical feedback was presented. In [31], a pseudorandom binary sequence was mixed within the chaotic dynamics in such a way that a mutual concealment was performed. In [32], Jing *et al.* reported an improved chaotic masking scheme based on the Lorenz system for secure communication. In [33], Liu, *et al.* proposed a chaotic secure communication method, namely, the partial series of a chaotic system for parameter estimation and the other series for secure communications. In [34], Wang, *et al.* developed a novel higher-dimensional digital chaotic system utilizing a chaos generation strategy controlled by random sequences. In [35], an experimental study of the practical realization of the transmission of information using chaotic oscillators was presented. In [36], a unified chaotic system and a hyperchaotic Rössler system with uncertain parameters were coupled, constrained and used as a new hyperchaotic system in a secure communication scheme. In [37], Oden, *et al.* proposed a chaotic communication scheme based on a chaotic optical phase carrier generated with an opto-electronic oscillator with nonlinear time-delay feedback. In [38], Chen, *et al.* initiated a systematic methodology for 6-D real domain chaos-based video encryption and decryption communications.

The above literatures are the application of chaos in secure communication, and then the literature [39] considers that a high dimensional model (map/ode system) is not a good choice for secure communication due to the scope of multistability. The authors think high-dimensional chaotic systems have more complex dynamic behaviors, better randomness and unpredictability. The high-dimensional chaotic system is used in the fields of secure communication, image encryption, text encryption and voice encryption, and will have a larger key space and higher security.. In [40], Sprott proposed the standard for constructing a new chaotic system, therefore, this paper proposes and introduces a new type of seven-dimensional hyperchaotic system. The proposed hyperchaotic system has satisfactory performance. It has only one control parameter and can be conveniently switched between hyperchaotic, chaotic, quasi-periodic, periodic, quasi-periodic and periodic states. Furthermore, the system parameters are large in scope, eliminating the risk of a sudden transition to an undesirable state. In view of chaos in some important fields, such as communication security and complex systems, the seven-dimensional hyperchaotic system is applied to signal encryption and decryption circuit design, and a physical circuit is tested to achieve secure communication.

II. CONSTRUCTION OF THE SEVEN-DIMENSIONAL HYPERCHAOTIC SYSTEM

In [41], a six-dimensional hyperchaotic system was proposed and defined by

$$\begin{cases} \dot{x} = a(y - x) + w - u - v \\ \dot{y} = cx - y - xz \\ \dot{z} = -bz + xy \\ \dot{w} = dw - yz \\ \dot{u} = ev + yz \\ \dot{v} = rx \end{cases} \tag{1}$$

where x, y, z, w, u, v are the system state variables and a, b, c, d, e, r are real coefficient, where dots indicate a derivative of time t.

The above system enters the hyperchaotic state when $a = 10, b = 8/3, c = 28, d = -1, e = 8, r = 3$. Based on this literature, we add a nonlinear controller $\dot{p}$ to the

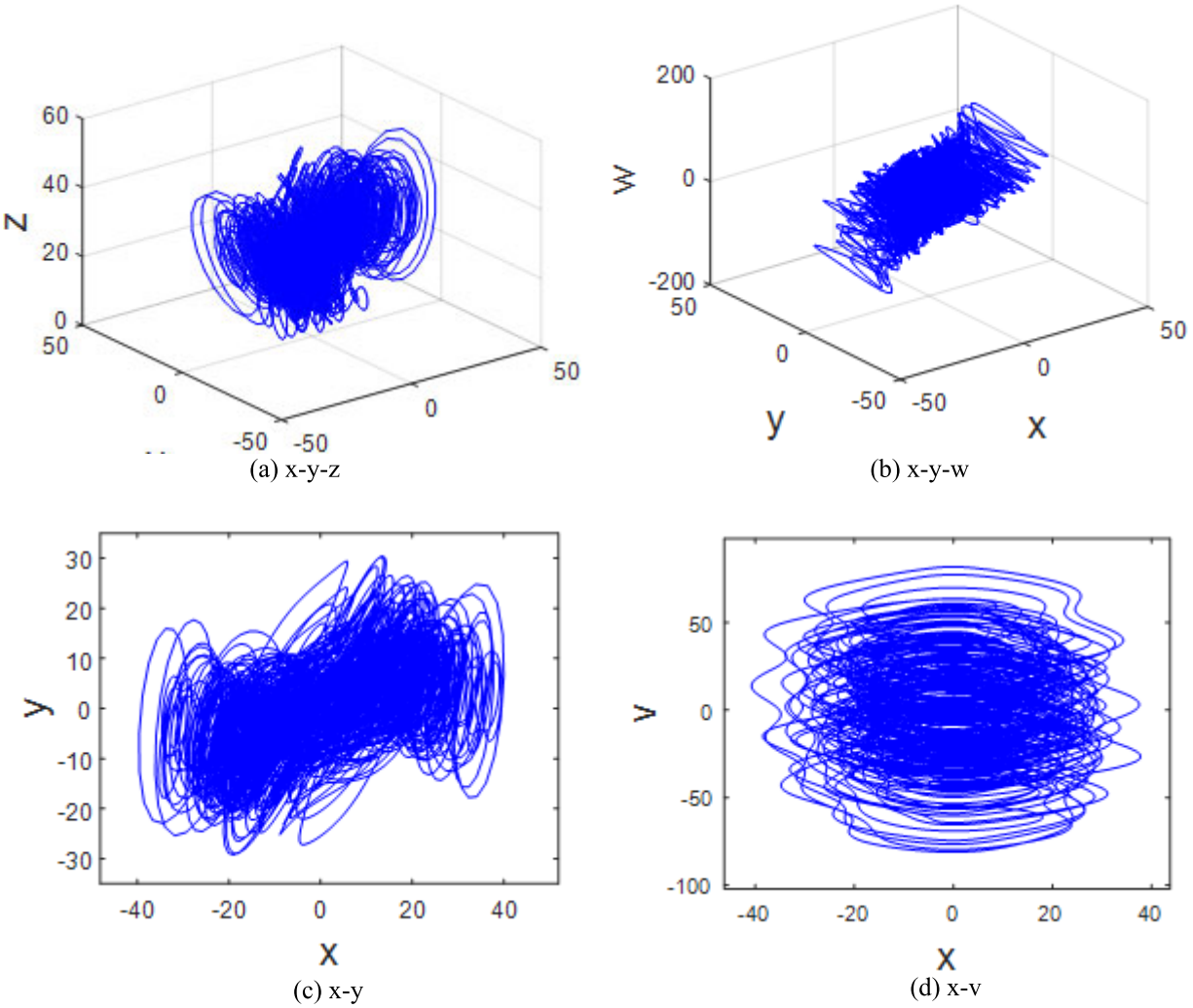

FIGURE 1. Hyperchaotic system phase diagrams for (a) x-y-z; (b) x-y-w; (c) x-y; and (d) x-v.

above system. The novel seven-dimensional hyperchaotic system is obtained as

$$\begin{cases} \dot{x} = a(y-x) + w - u - v \\ \dot{y} = cx - y - xz - p \\ \dot{z} = -bz + xy \\ \dot{w} = dw - yz \\ \dot{u} = ev + yz \\ \dot{p} = fx + yz \\ \dot{v} = rx \end{cases} \tag{2}$$

From Ref. [17], regarding the hyperchaotic system, some principles need to be satisfied: (1) the system should have dissipativity; (2) the dimension of the system should be at least 4; and (3) the system should have at least two equations that enhance the instability, and the two equations should have at least one nonlinear term.

Here, if $a = 10, b = 8/3, c = 28, d = -1, e = 8, f = 1, r = 5$, then the Lyapunov exponents are

$$L_1 = 0.58845,\ L_2 = 0.178183,\ L_3 = 0,\ L_4 = -0.139483,$$
$$L_5 = -0.404591,\ L_6 = -0.80156,\ L_7 = -14.088129$$

At this point, the Lyapunov exponent of the system has two positive, one zero and five negative. The sum of all Lyapunov exponents is $L = -13.86557$, obviously, it is less than zero. Therefore, the system is now in a hyperchaotic state. The related phase portraits between x, y, z, w and v are shown in Fig. 1.

In Fig. 1, (a), (b), (c), and (d) correspond to the phase diagrams of the attractors for x-y-z, x-y-w, x-y, and x-v, respectively.

III. THEORETICAL ANALYSIS OF THE PROPOSED HYPERCHAOTIC SYSTEM

Compared to chaotic systems, hyperchaotic systems have the following advantages. First, two or more of the

Lyapunov exponents of the hyperchaotic system are greater than zero. Second, its dynamic behavior is more complicated and the phase trajectories are separated in more directions. Based on this, hyperchaotic signals can improve the security of chaotic information encryption and chaotic secure communication.The dynamic behavior of the hyperchaotic system is analyzed as follows: the stability and balance analysis of the hyperchaotic system is first demonstrated, and then the dissipation of the system is verified. Finally, the proposed system is analyzed by the bifurcation diagram and the Lyapunov exponent spectrum.

A. STABILITY, EQUILIBRIUM AND DISSIPATIVITY

1) STABILITY AND EQUILIBRIUM

As introduced above, the equations of stability are

$$\begin{cases} a(y-x)+w-u-v=0 \\ cx-y-xz-p=0 \\ -bz+xy=0 \\ dw-yz=0 \\ ev+yz=0 \\ fx+yz=0 \\ rx=0 \end{cases} \tag{3}$$

Solving the system of equations (3), the equilibrium point $O(0, y^*, 0, 0, ay^*, -y^*, 0)$, $y^* \in R$ can be obtained, which is independent of the value of the parameters b, c, d, e, f, r. The Jacobian matrix of system (2) at the equilibrium point O is

$$J = \begin{bmatrix} -a & a & 0 & 1 & -1 & 0 & -1 \\ c & -1 & 0 & 0 & 0 & -1 & 0 \\ y^* & 0 & -b & 0 & 0 & 0 & 0 \\ 0 & 0 & -y^* & d & 0 & 0 & 0 \\ 0 & 0 & y^* & 0 & 0 & 0 & e \\ f & 0 & y^* & 0 & 0 & 0 & 0 \\ r & 0 & 0 & 0 & 0 & 0 & 0 \end{bmatrix} \tag{4}$$

As $|J-\lambda I|=0$, the characteristic equation is:

$$\begin{aligned} &-\lambda^7+[(d-a-1)\lambda^6 \\ &+[(c+d-b-1)a+b(d-1)+d-r]\lambda^5 \\ &+[(d-b-f+bc+bd\text{-cd})a-(1+b+e-d)r-2y^{*2}] \\ &\lambda^4+[(bd-bf+df-bcd)a+(dr-er-r)b+er \\ &(d-1)+dr+y^{*2}(d-a-2)] \\ &\lambda^3+[(dr+br+bdf)a+er(d-b+bd)+dy^{*2}(a+1)] \\ &\lambda^2+bder\lambda=0 \end{aligned}$$

When $y^*=0$, the characteristic equation change as:

$$\begin{aligned} \lambda(d-\lambda)(\lambda+b)[\lambda^4+(a+1)\lambda^3+(a+r)\lambda^2 \\ +(af+r-er-acf)\lambda-er]=0 \end{aligned} \tag{5}$$

When $a=10, b=8/3, c=28, d=-1, e=8, f=1, r=5$, the seven eigenvalues are

$$\begin{aligned} &\lambda_1=11.534686,\ \lambda_2=0.513269,\ \lambda_3=-2.66667, \\ &\lambda_4=0,\ \lambda_5=-0.29768,\ \lambda_6=-1,\ \lambda_7=-22.750328 \end{aligned}$$

Obviously, two eigenvalues are positive, one eigenvalue is zero and the others are negative. It can be concluded that O is an unstable saddle point when $y^*=0$.

2) DISSIPATIVITY

Assuming ψ is a region in the smooth surface R^7 and $V(t)$ is the volume of $\psi(t)$. We obtain

$$\dot{V}(t)=\int_{\psi(t)}\left(\nabla^* V\right)dxdydzdwdudpdv. \tag{6}$$

Through equation (6), we can calculate the dissipation of hyperchaotic systems.

$$\begin{aligned} \nabla^* V &= \frac{\partial \dot{x}}{x}+\frac{\partial \dot{y}}{y}+\frac{\partial \dot{z}}{z}+\frac{\partial \dot{w}}{w}+\frac{\partial \dot{u}}{u}+\frac{\partial \dot{p}}{p}+\frac{\partial \dot{v}}{v} \\ &= -a-1-b+d=\gamma \end{aligned} \tag{7}$$

where V is the seven-dimensional hyperchaotic system and a, b, c, d, e, f and r are real parameters. The above equation is rewritten as

$$\dot{V}(t)=\int_{\psi(t)}\gamma\, dxdydzdwdudpdv=\gamma V(t). \tag{8}$$

Therefore, we can obtain $V(t)=e^{\gamma}V(0)$, if $\nabla^* V<0$, then system (2) is dissipative, and the state of the system is bounded by the state of the system. When $a=10, b=8/3, c=28, d=-1, e=8, f=1, r=5, \gamma=-\frac{44}{3}<0$, a volume element for the initial $V(0)$ gradually converges to $V(0)e^{-\frac{44}{3}t}$ at time t. When $t\to\infty$, every trajectory of the system converges to 0 with a rate of $-\frac{44}{3}$. Eventually, as all system trajectories will eventually be limited to a set of zero volumes, the progressive motion of the system will be fixed at the attractors.

B. BIFURCATION AND THE LYAPUNOV EXPONENT SPECTRUM

Bifurcation is a kind of special nonlinear phenomenon related to hyperchaos, chaos and mutation. The common way to obtain bifurcation is with the maximum of a parameter. For hyperchaos and chaos, the Lyapunov exponents are essential, which indicate a diverging rate of trajectory. In addition, the Lyapunov exponents is a useful tool to analyse and judge hyperchaos. For our proposed 7D hyperchaotic system, the bifurcation diagram and the Lyapunov exponent spectrum with linear control coefficients $r\in[0, 90]$ (The other parameters are fixed at $a=10, b=8/3, c=28, d=-1, e=8, f=1$) and an initial condition $(x_0, y_0, z_0, w_0, u_0, p_0, v_0)=(1,1,1,1,1,1,1)$ are shown in Fig. 2. At the same time, the three largest Lyapunov exponents of the 7D hyperchaotic system are shown in Fig2(c).

As illustrated above Fig. 2(a), when the nonlinear coefficient r is increased, Xmax varies from an unstable to a stable status, and bifurcation clearly occurs. In Fig. 2(b), the Lyapunov exponent L1 varies from positive values to zero and then to negative values, and L2 drops from a positive

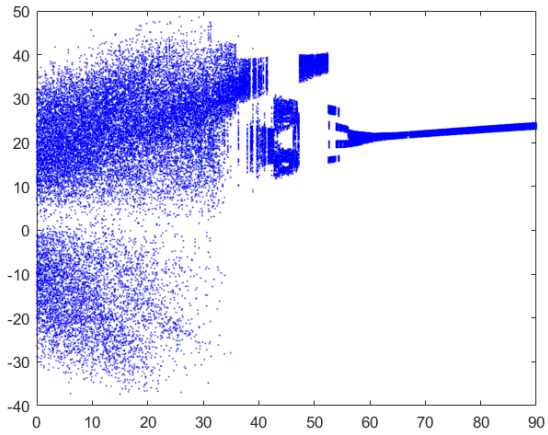

(a) bifurcation diagram

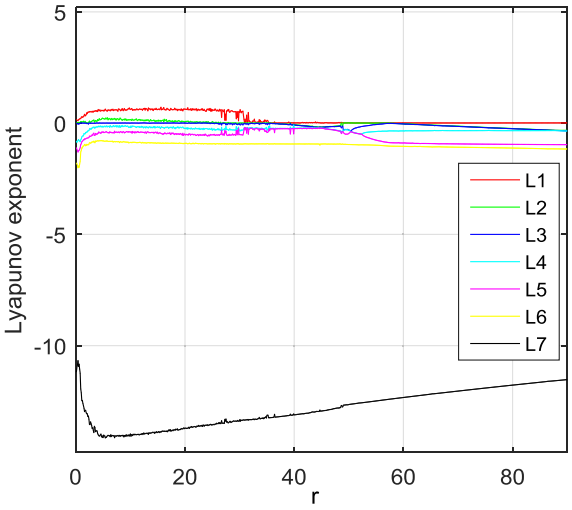

(b) Lyapunov exponent spectrum

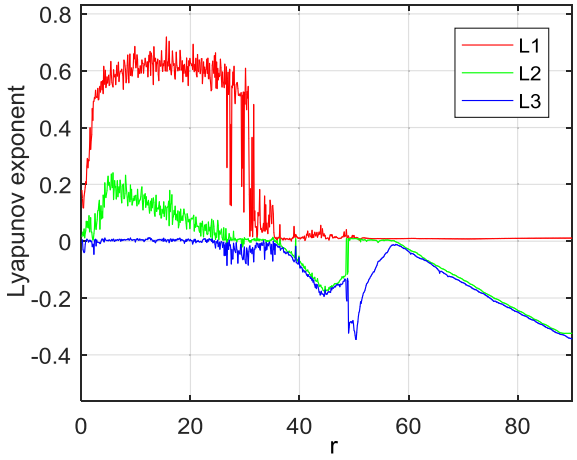

(c) The main Lyapunov exponents

FIGURE 2. Systematic bifurcation diagram and the Lyapunov exponent spectrum: (a) bifurcation diagram; (b) Lyapunov exponent spectrum; (c) The main Lyapunov exponents.

value to a negative value, then mutates to zero and finally decreases to a negative value. This indicates that with an increase in the nonlinear control coefficient r, the positive maximum Lyapunov exponent L1 tends to decrease linearly, and L2 tends to decrease linearly at first, but when the linear control coefficient r increases to 49, L2 suddenly increases to zero and then decreases linearly. Accordingly, the condition of the proposed seven-dimensional hyperchaotic system changes from hyperchaotic, chaotic, quasi-periodic attraction, periodic attraction, quasi-periodic attraction to periodic attraction.

To estimate the validity of our proposed seven-dimensional hyperchaotic system, six nonlinear states are introduced in detail. When $0 < r < 25.5$, the system has two positive Lyapunov exponents, and the system is in a hyperchaotic state. When $25.5 < r < 31.82$, the system has a positive Lyapunov exponent, and the system is in a chaotic state. When $31.82 < r < 35.8$, the system is in a quasi-periodic state. When $35.8 < r < 49$, the system is in a periodic state. When $49 < r < 57.6$, the system resumes to a quasi-periodic state. When $57.6 < r < 90$, the system is in a periodic state.

1) HYPERCHAOS

Hyperchaos has more complex features than common chaos due to the presence of multiple attractors. As shown in Fig. 2, hyperchaos occurs in our proposed seven-dimensional hyperchaotic system when $0 < r < 25.5$. The phase diagrams of x-y, x-z, y-z and x-w are shown in Fig. 3. To show its chaotic character further, the 3D projections of phase diagram are also shown in Fig. 3(e) and Fig. 3(f). It is known that hyperchaos exists in the system when at least two Lyapunov exponents are positive. According to the calculation, the seven Lyapunov exponents are $L_1 = 0.58845, L_2 = 0.178183, L_3 = 0, L_4 = -0.139483, L_5 = -0.404591, L_6 = -0.801560, L_7 = -14.088129$.

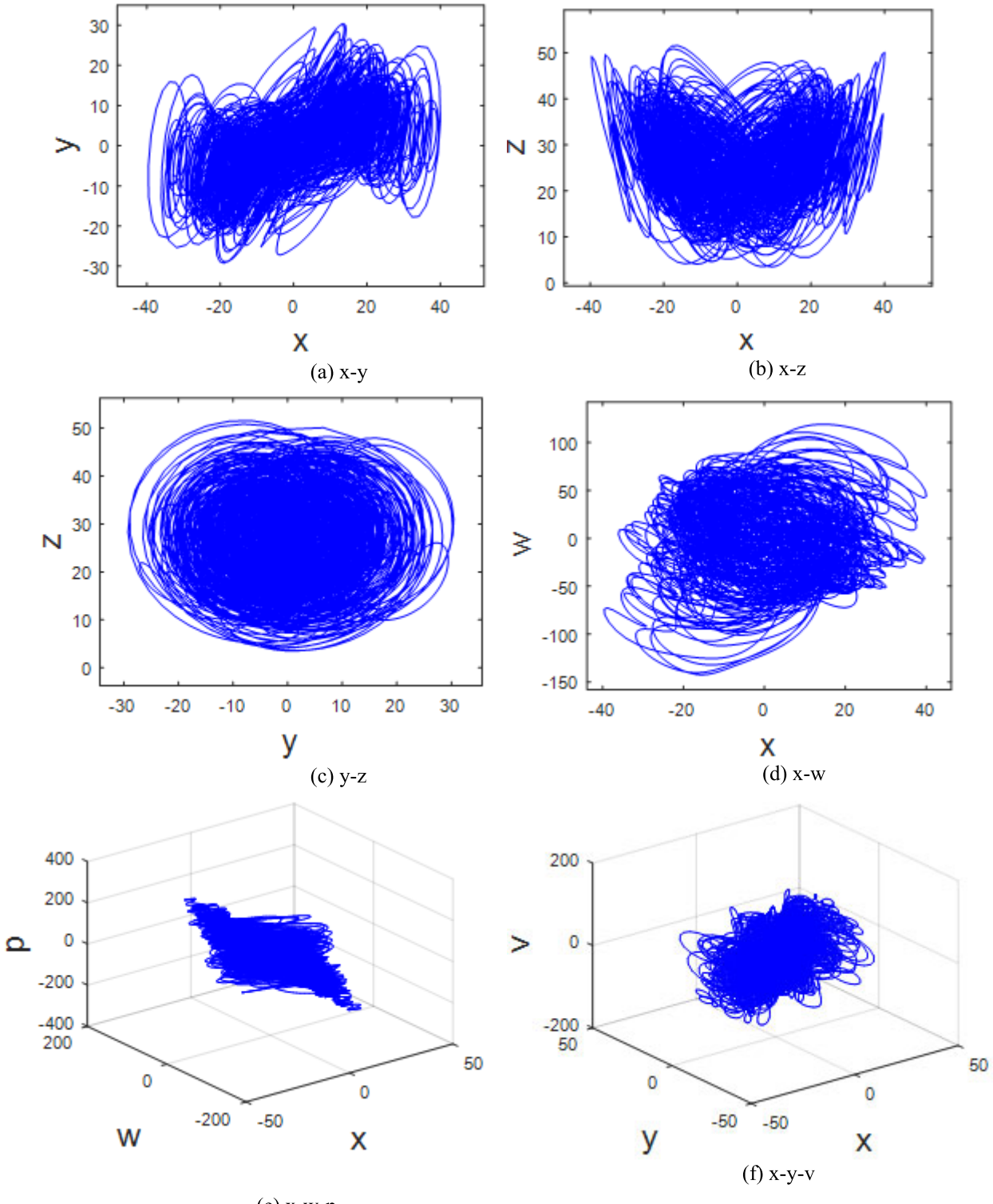

FIGURE 3. Phase diagram of the system when $r = 5$: (a) x-y; (b) x-z; (c) y-z; (d) x-w; (e) x-w-p; and (f) x-y-v.

Obviously, two maximum Lyapunov exponents are positive, and the sum of the Lyapunov exponents is $-14.663665<0$. According to above explanations, the proposed seven-dimensional hyperchaotic system is in a hyperchaotic state when the nonlinear coefficient $r = 5$.

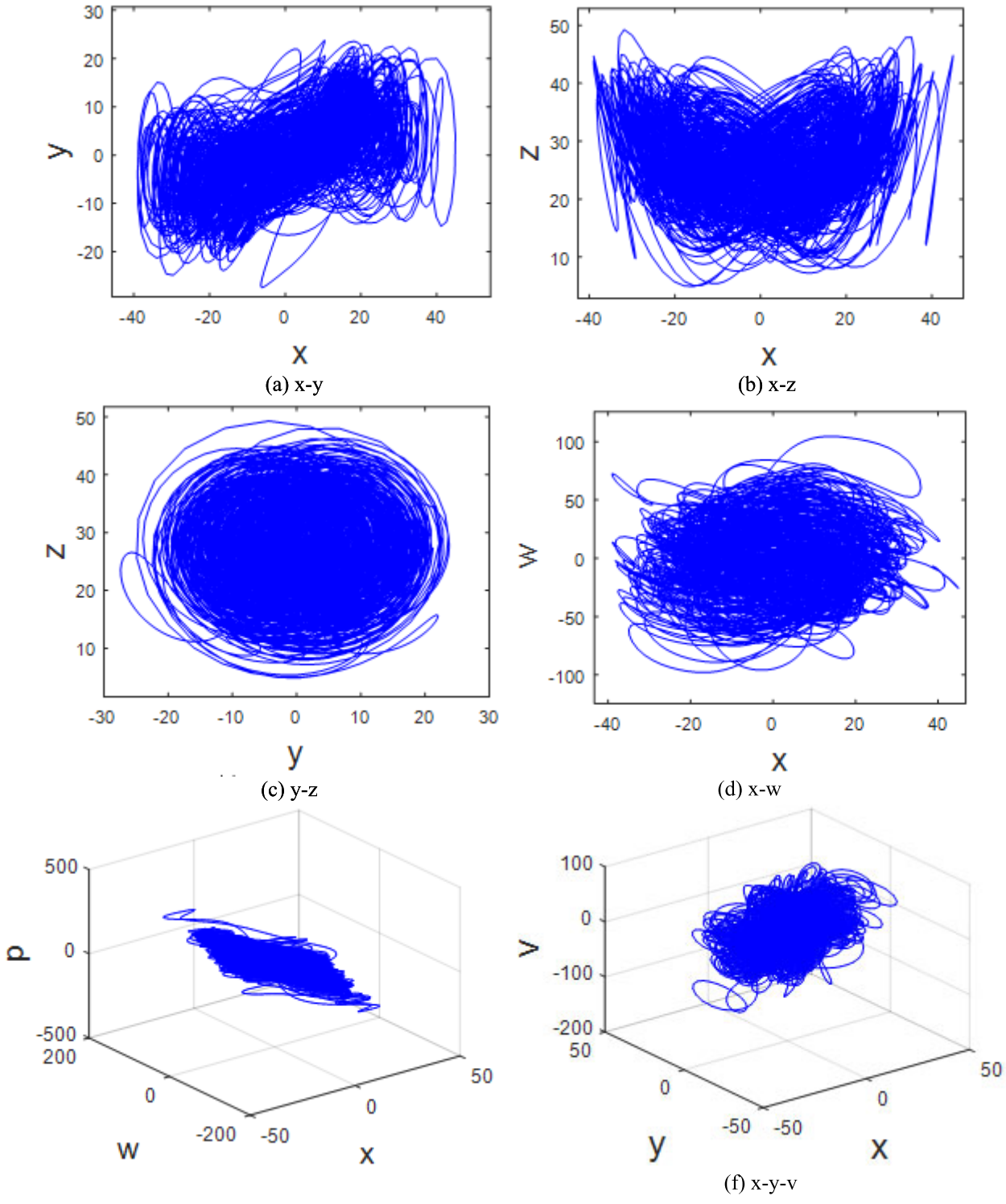

FIGURE 4. Phase diagram of the system when r = 30: (a) x-y; (b) x-z; (c) y-z; (d) x-w; (e) x-w-p; and (f) x-y-v.

2) CHAOS

As shown from the bifurcation, a chaotic phenomenon clearly appears when $25.5 < r < 31.82$. The phase diagrams of x-y, x-z, y-z and x-w are shown in Fig. 4. To show its chaotic character further, the 3D projections of phase diagram are also shown in Fig. 4(e) and Fig. 4(f).

According to the calculation, the seven Lyapunov exponents are: $L_1 = 0.390444, L_2 = -0.002648, L_3 = -0.057088, L_4 = -0.279529, L_5 = -0.449534, L_6 = -0.932220, L_7 = -13.336128$.

The sum is -14.60715. Compared with the above hyperchaotic system, obviously, only one Lyapunov exponent is positive, and the others are zero or negative. It can be concluded that the system now exhibits a chaotic state when the nonlinear coefficient $r = 30$.

3) QUASI-PERIODIC ATTRACTION

When the linear control parameter is continuously increased, the seven-dimensional hyperchaotic system is changed to a quasi-periodic state. The dynamic behaviour of the proposed system maintains the quasi-period state when $31.82 < r < 35.8$. When $r = 35.5$, the dynamic behaviour of the proposed system is that of the quasi-periodic attractor state. Similarly, the Lyapunov exponents are $L_1 = 0, L_2 = 0, L_3 = -0.05355, L_4 = -0.09956, L_5 = -0.34054, L_6 = -0.93871, L_7 = -13.22658$.

The related phase portraits of the system parameters are shown in Fig. 5(a), Fig. 5(b), Fig. 5(c) and Fig. 5(d). In Fig. 5(e) and Fig. 5(f), the 3D projections of phase diagram are also shown to show its chaotic character further. According to the above introductions, the proposed seven-dimensional hyperchaotic system changes from a chaotic state to a periodic attraction state.

4) PERIODIC ATTRACTION

When $35.8 < r < 49$, the system is in a state of periodic attraction. Therefore, the related phase portraits in the system are explained in Fig. 6(a), Fig. 6(b), Fig. 6(c) and Fig. 6(d) with $r = 49$. Simultaneously, in Fig. 6(e) and Fig. 6(f), the 3D projections of phase diagram are also shown to show its chaotic character further. According to the calculation, the Lyapunov and exponents are $L_1 = 0, L_2 = -0.081799, L_3 = -0.082942, L_4 = -0.228819, L_5 = -0.230043, L_6 = -0.936582, L_7 = -13.107841$.

The sum is $-14.668026<0$. Obviously, the system is now in a periodic attraction state.

5) QUASI-PERIODIC ATTRACTION

When the linear parameter r increases to 49, the Lyapunov exponent L_2 changes from a negative value to zero, causing the system to return from the periodic state to the quasi-periodic state. The related phase portraits in the system are explained in Fig. 7(a), Fig. 7(b), Fig. 7(c) Fig. 7(d) with $r = 50$. Simultaneously, in Fig. 7(e) and Fig. 7(f), the 3D projections of phase diagram are also shown to show its chaotic character further. The seven Lyapunov exponents of the system are $L_1 = 0, L_2 = 0, L_3 = -0.30887, L_4 = -0.309484, L_5 = -0.45356, L_6 = -0.96081, L_7 = -12.63748$.

6) PERIODIC ATTRACTION

When the linear parameter r increases to 57.6, the system enters the periodic state. When $57.6 < r < 90$, the system has a period-invariant state. When $r = 80$, the related phase portraits in the system are explained in Fig. 8(a), Fig. 8(b), Fig. 8(c). and Fig. 8(d). Simultaneously, in Fig. 8(e) and Fig. 8(f), the 3D projections of phase diagram are also shown to show its chaotic character further. According to the calculation, the Lyapunov exponents are: $L_1 = 0, L_2 = -0.248482, L_3 = -0.249183, L_4 = -0.334730, L_5 = -0.950542, L_6 = -1.119606, L_7 = -11.765346$.

Obviously, the system is now in a state of periodic attraction.

C. COMPLEXITY ANALYSIS

The complexity of chaotic systems refers to the degree to which chaotic sequences are close to random sequences using correlation algorithms. The greater the complexity value, the more difficult it is for the sequence to be restored to the original sequence, and the corresponding security is higher. Algorithm complexity can be generally divided into behavior-based complexity algorithms (FuzzyEn algorithm and LMC algorithm) and structural complexity-based algorithms (SE complexity algorithm and C_0 complexity algorithm).

At present, there are many algorithms for calculating the behavioral complexity of chaotic pseudo-random sequences, which are based on the Kolmogorov method and Shannon entropy. Such algorithms are fast and accurate. However, it does not apply to pseudo-random sequences with high dimensionality. Therefore, here we use the C_0 complexity algorithm.

The complexity of different dimensions of the system when the parameter r changes is calculated separately, and the result is shown in Fig. 9. When calculating the complexity, the calculation step is 0.05s, and the sequence length is 50000. The complexity decreases with the increase of r value and is consistent with Figure 2(b). It can be seen that the C_0 complexity can reflect the system. Dynamic characteristics. When $0 < r < 25.5$, it can be clearly seen that C_0 complexity is greater than other moments. At this time, the system has two positive Lyapunov exponents, which are in hyperchaotic state. When $25.5 < r < 31.82$, the C_0 complexity has decreased, but it is still significantly greater than zero. At this point the system has a positive Lyapunov exponent, in a chaotic state. At $r > 31.82$, the C_0 complexity gradually approaches 0 and eventually tends to zero. At this point, the system does not have a positive Lyapunov exponent, lingering between the quasi-period and the cycle.

IV. THE CIRCUIT REALIZATION OF THE SEVEN-DIMENSIONAL HYPERCHAOTIC SYSTEM.

Circuit verification of the proposed hyperchaotic system is a crucial step to ensure its correctness. Furthermore, the key issue in circuit implementation is how to transform the theoretical expression of the seven-dimensional hyperchaotic system into a realistic circuit expression using electronic devices,

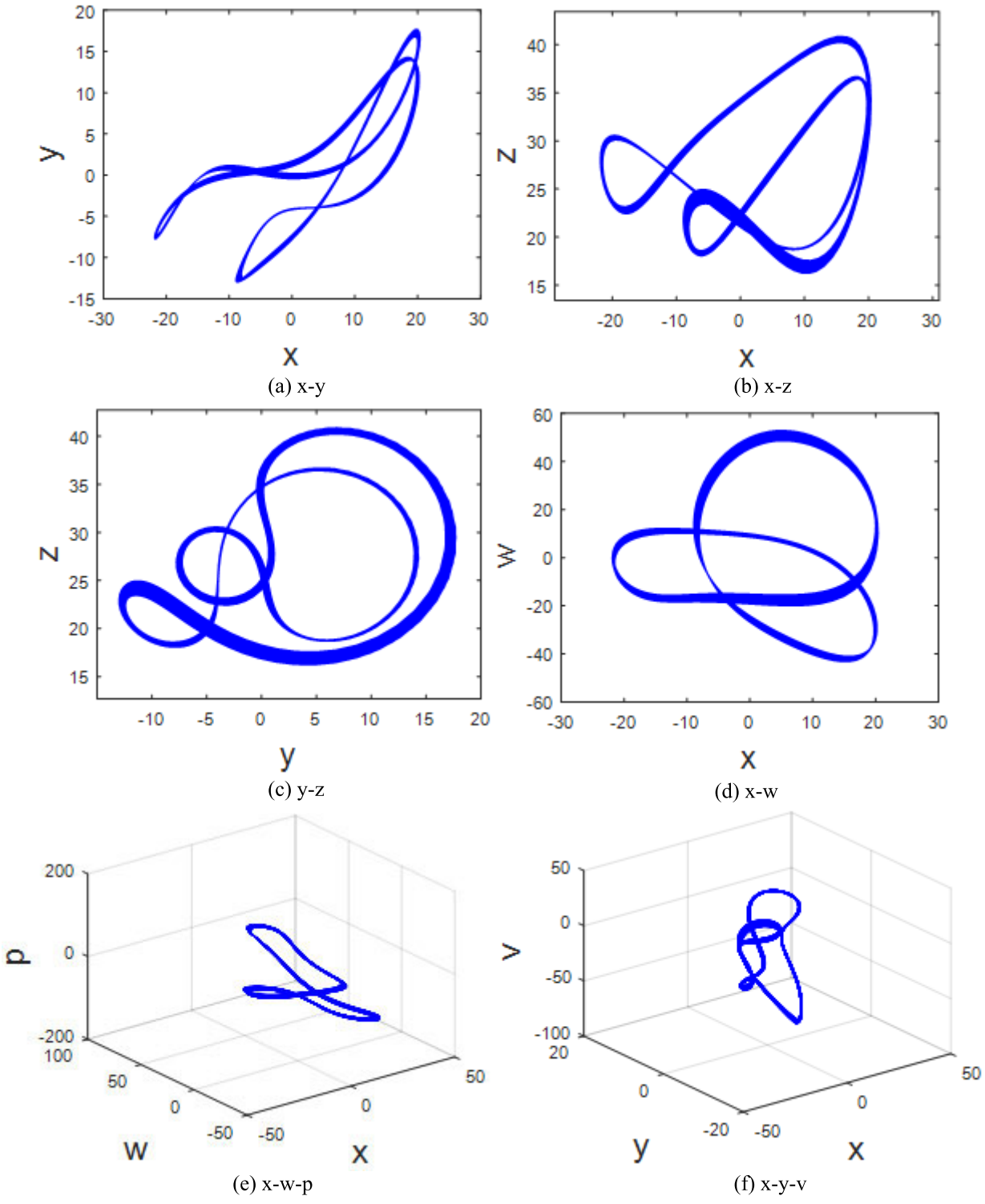

FIGURE 5. Phase diagram of the system when $r = 35.5$: (a) x-y; (b) x-z; (c) y-z; (d) x-w; (e) x-w-p; and (f) x-y-v.

such as resistors and capacitors. To verify the effectiveness of the seven-dimensional hyperchaotic system, a circuit implementation is designed and simulated using the circuit simulation software NI Multisim (ver. 2014), and the simulation results are also explained in detail in this section. Only the processes that verify the system effectiveness when the system is in a state of hyperchaos are listed here.

In Sec. 2, we propose a seven-dimensional hyperchaotic system. This paper only discusses the process of verifying the system validity when $r = 5$.

Because of the large dynamic range of system variables, it is necessary to perform a proportional compression transformation for better display on an oscilloscope. After uniformly compressing 10 times, the parameters are substituted into equation (2).

$$\begin{cases} \dot{x} = 10(y - x) + w - u - v \\ \dot{y} = 28x - y - 10xz - p \\ \dot{z} = -8/3z + 10xy \\ \dot{w} = -1w - 10yz \\ \dot{u} = 8v + 10yz \\ \dot{p} = 1x + 10yz \\ \dot{v} = 5x \end{cases} \tag{9}$$

To facilitate the observation of the operation result of the circuit on the oscilloscope, it is also necessary to change the time step of the model for a time scale conversion. Letting $\tau = \tau_0 t$, $\tau_0 = 100$, We find

$$\begin{cases} \dot{x} = -1000x - 1000(-y) - 100(-w) \\ -100u - 100v \\ \dot{y} = -2800(-x) - 100y - 1000xz - 100p \\ \dot{z} = -800/3z - 1000(-x)y \\ \dot{w} = -100w - 1000yz \\ \dot{u} = -800(-v) - 1000(-y)z \\ \dot{p} = -100(-x) - 1000(-y)z \\ \dot{v} = -500(-x) \end{cases} \tag{10}$$

The approximation expression of the hyperchaotic system can be obtained by using adders, integrators, multipliers and inverters. However, the accuracy of its circuit simulation and experimental results cannot be met. Therefore, the improved chaotic circuit module design is adopted. The related circuit implementation is shown in Fig. 9. Moreover, these circuits consist of resistors, capacitors, the analogy multiplier AD633 with $\pm 15V$, and the operational amplifier TL085 with $\pm 35V$.

The chaotic circuit of this system is shown in Fig. 9. The parameters of each component are given in the circuit diagram. Based on Kirchhoff's law, Ohm's law, the virtual short circuit, the virtual open circuit and the reverse integration circuit, the following expression can be obtained.

$$\begin{cases} \dot{x} = -\dfrac{R_7}{C_1R_1R_6}x - \dfrac{R_7}{C_1R_2R_6}(-y) - \dfrac{R_7}{C_1R_3R_6}(-w) \\ \quad -\dfrac{R_7}{C_1R_4R_6}u - \dfrac{R_7}{C_1R_5R_6}v \\ \dot{y} = -\dfrac{R_{13}}{C_2R_8R_{12}}(-x) - \dfrac{R_{13}}{C_2R_9R_{12}}y - \dfrac{R_{13}}{C_2R_{10}R_{12}} \\ \quad xz - \dfrac{R_{13}}{C_2R_{11}R_{12}}p \\ \dot{z} = -\dfrac{R_{17}}{C_3R_{14}R_{16}}z - \dfrac{R_{17}}{C_3R_{15}R_{16}}(-x)y \\ \dot{w} = -\dfrac{R_{21}}{C_4R_{18}R_{20}}w - \dfrac{R_{21}}{C_4R_{19}R_{20}}yz \\ \dot{u} = -\dfrac{R_{25}}{C_5R_{22}R_{24}}(-v) - \dfrac{R_{25}}{C_5R_{23}R_{24}}(-y)z \\ \dot{p} = -\dfrac{R_{29}}{C_6R_{26}R_{28}}(-x) - \dfrac{R_{29}}{C_6R_{27}R_{28}}(-y)z \\ \dot{v} = -\dfrac{R_{32}}{C_7R_{30}R_{31}}(-x) \end{cases} \tag{11}$$

The chaotic circuit of this system is shown in Fig. 10. The parameters of each component are given in the circuit diagram. Based on Kirchhoff's law, Ohm's law, the virtual short circuit, the virtual open circuit and the reverse integration circuit, the following expression can be obtained. Combining equations (10) and (11), when the values of the capacitors are taken as $C_1 = C_2 = C_3 = C_4 = C_5 = C_6 = C_7 = 10\text{nF}$, the values of all the resistors can be found as:

$R_1 = 100\text{k}\Omega$, $R_2 = 100\text{k}\Omega$, $R_3 = 1000\text{k}\Omega$,
$R_4 = 1000\text{k}\Omega$, $R_5 = 1000\text{k}\Omega$,
$R_6 = 100\text{k}\Omega$, $R_7 = 100\text{k}\Omega$, $R_8 \approx 35.712\text{k}\Omega$,
$R_9 = 1000\text{k}\Omega$, $R_{10} = 10\text{k}\Omega$,
$R_{11} = 1000\text{k}\Omega$, $R_{12} = 100\text{k}\Omega$,
$R_{13} = 100\text{k}\ \Omega$, $R_{14} = 375\text{k}\Omega$, $R_{15} = 10\text{k}\Omega$,
$R_{16} = 100\text{k}\Omega$, $R_{17} = 100\text{k}\Omega$,
$R_{18} = 1000\text{k}\ \Omega$, $R_{19} = 10\text{k}\Omega$, $R_{20} = 100\text{k}\Omega$,
$R_{21} = 100\text{k}\Omega$, $R_{22} = 125\text{k}\Omega$,
$R_{23} = 10\text{k}\Omega$, $R_{24} = 100\text{k}\Omega$, $R_{25} = 100\text{k}\Omega$,
$R_{26} = 1000\text{k}\Omega$, $R_{27} = 10\text{k}\Omega$, $R_{28} = 100\text{k}\Omega$,
$R_{29} = 100\text{k}\Omega$, $R_{30} = 200\text{k}\Omega$, $R_{31} = 100\text{k}\Omega$, $R_{32} = 100\text{k}\Omega$.

After the circuit simulation is implemented, the relevant phase diagram of the state variables in the circuit is shown in Fig. 11. The two attractors of x-y appear clearly in Fig. 11(a), and the phase portraits such as the butterfly portrait of x-z, are easily recognized in Fig. 11(b), which are similar to those in Fig. 3(a) and Fig. 3(b). Furthermore, the phase portraits, such as the circles of y-z, are identical to those in Fig. 3(c). In addition, the phase pattern $y - z$ in Fig. 11(c) resembles a circle, which is the same as in Fig. 3(c). The phase pattern of Fig. 11(d) is a sphere that is somewhat

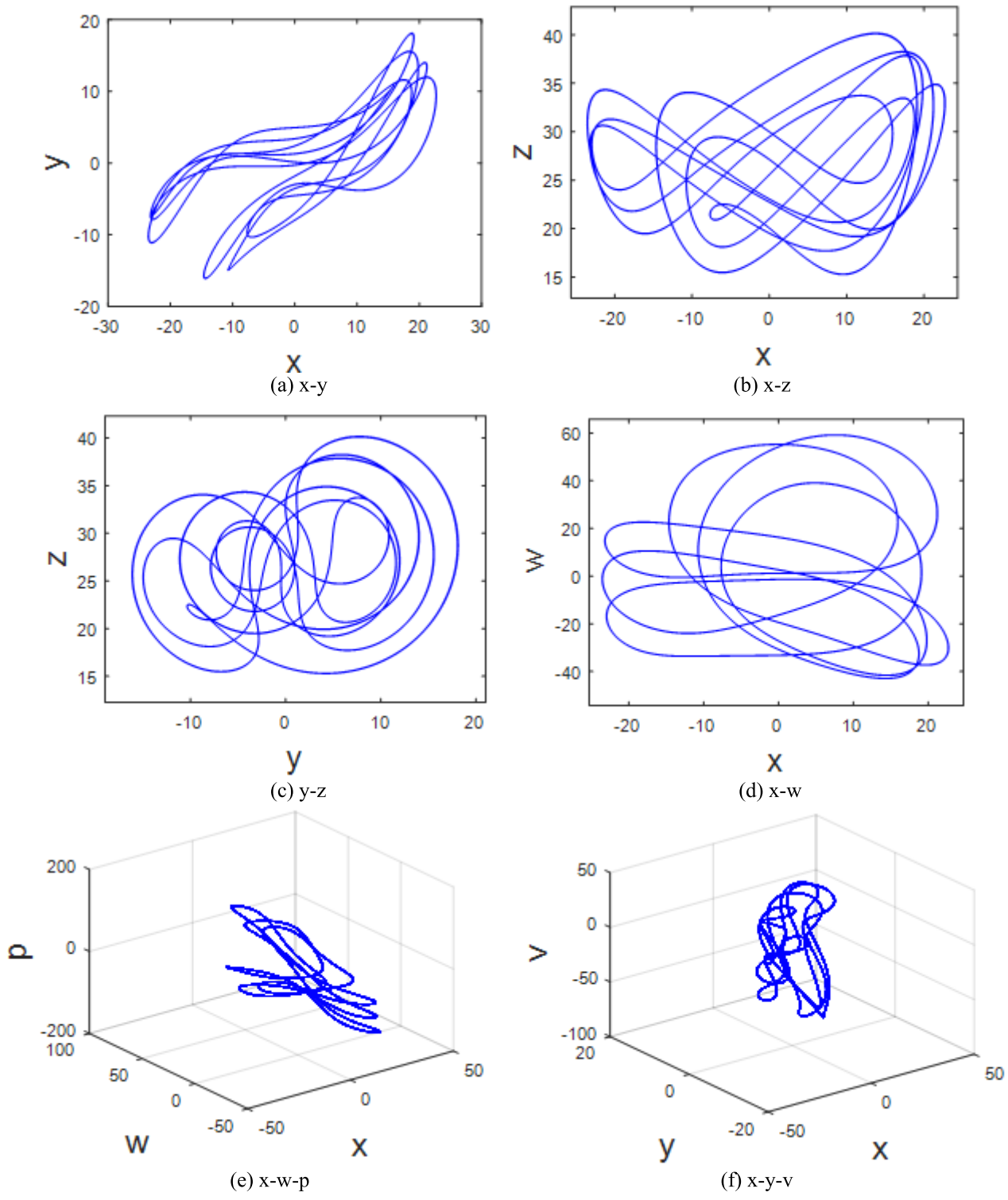

(a) x-y (b) x-z (c) y-z (d) x-w (e) x-w-p (f) x-y-v

FIGURE 6. Phase diagram of the system when $r = 40$: (a) x-y; (b) x-z; (c) y-z; (d) x-w; (e) x-w-p; and (f) x-y-v.

divergent at the upper and lower ends, similar to the phase diagram in Fig. 3(d). The results indicate the correctness and validity of the proposed hyperchaotic system, demonstrating that our proposed seven-dimensional hyperchaotic system indeed generates hyperchaotic phenomena using the given parameters.

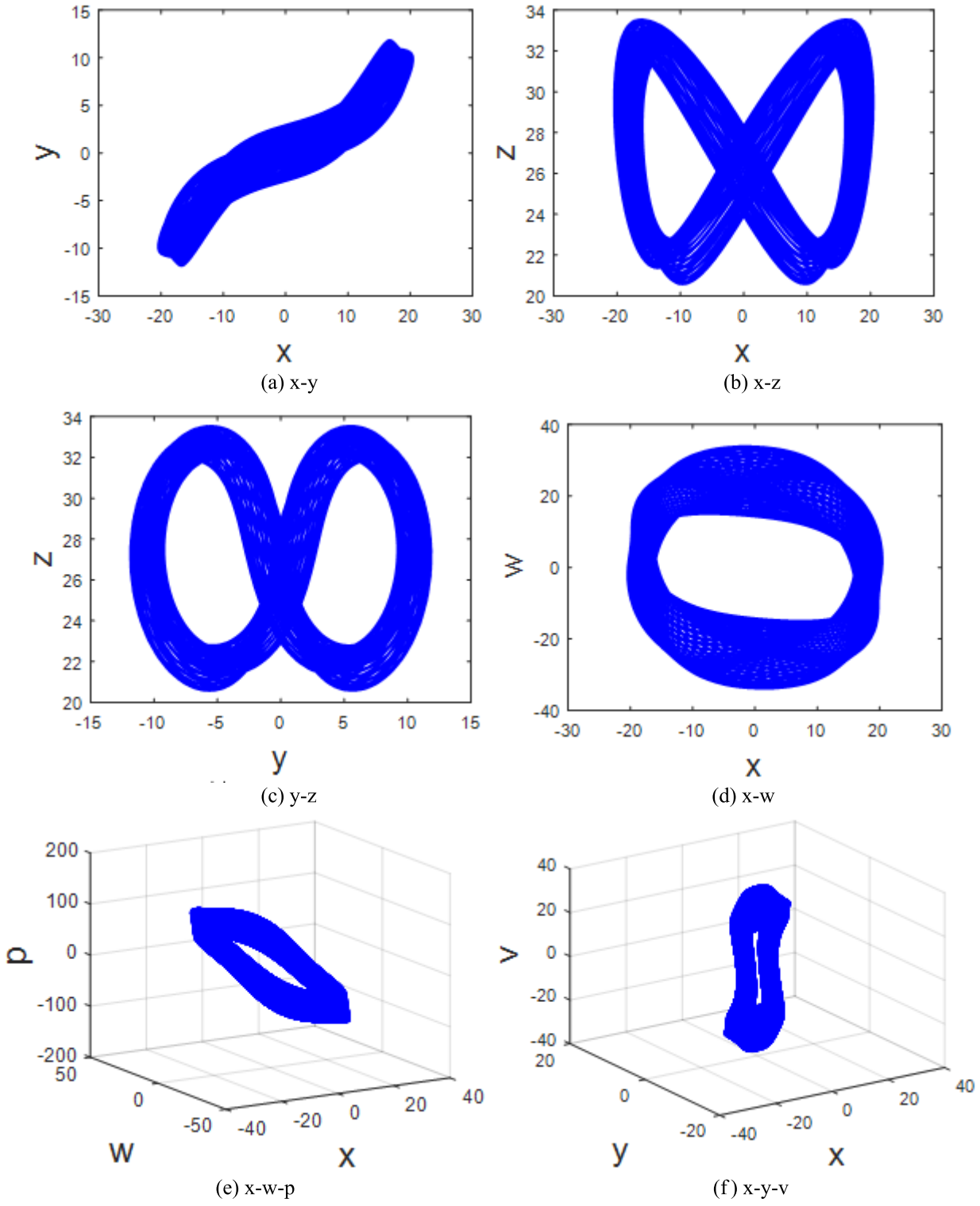

FIGURE 7. Phase diagram of the system when $r = 50$: (a) x-y; (b) x-z; (c) y-z; (d) x-w; (e) x-w-p; and (f) x-y-v.

V. APPLICATION OF CHAOTIC SYSTEM IN SECURE COMMUNICATION

A. CHAOTIC SYNCHRONIZATION

Chaotic synchronization can realize the complete reconstruction of the chaotic state of the two systems. In general, it belongs to the category of chaos control. At the same time, chaotic synchronization is the key to realize chaotic secure communication. Chaotic synchronization can be realized, making chaotic communication possible. Common methods for implementing chaotic synchronization include

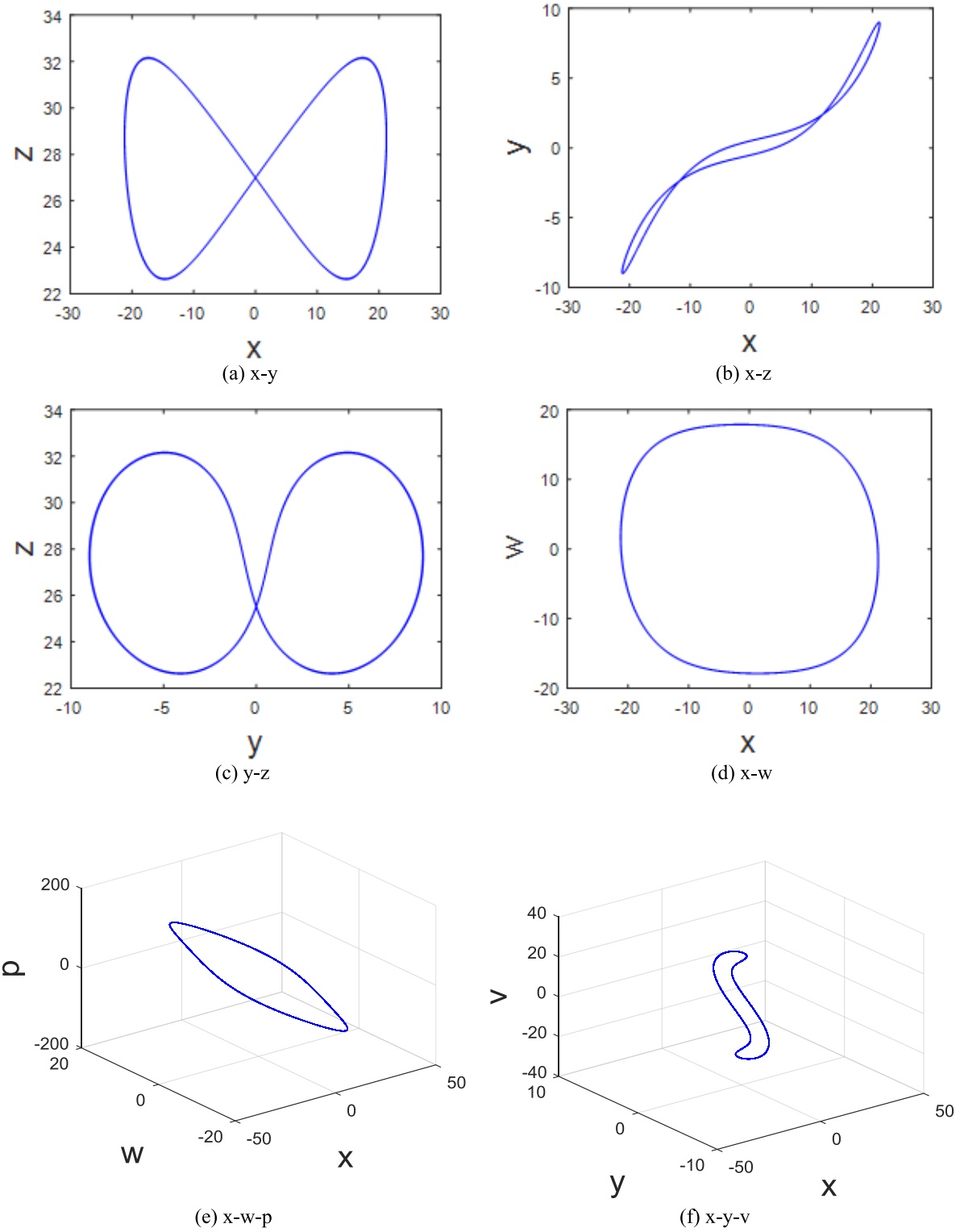

FIGURE 8. Phase diagram of the system when $r = 80$: (a) x-y; (b) x-z; (c) y-z; (d) x-w; (e) x-w-p; and (f) x-y-v.

adaptive synchronization, coupled synchronization, pulse synchronization, and drive response synchronization. Among them, the driver response synchronization has the advantages of good compatibility, strong self-synchronization and only one encryption. Inspired by the literature [42]–[44], driver response synchronization

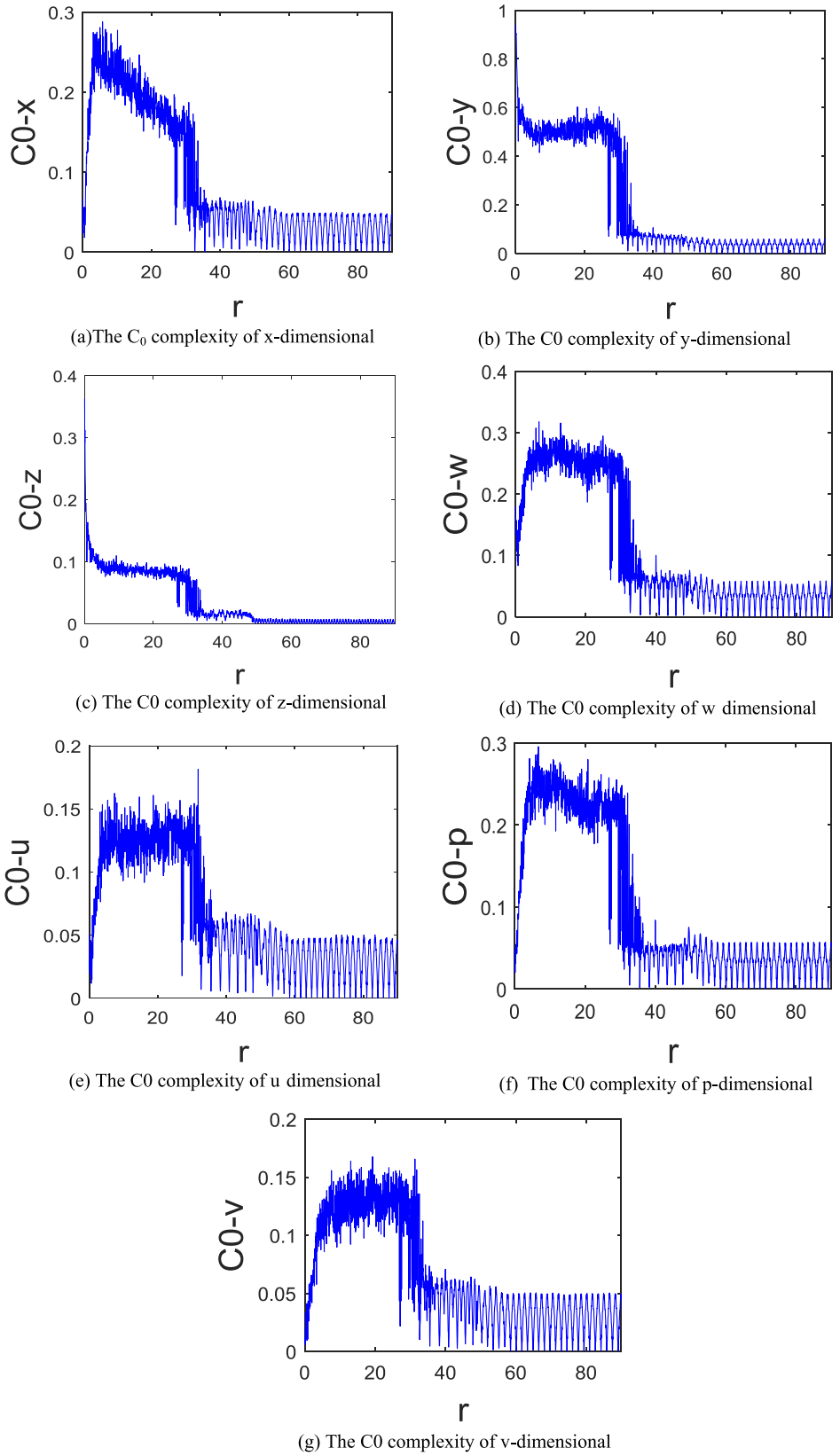

(a)The C_0 complexity of x-dimensional

(b) The C0 complexity of y-dimensional

(c) The C0 complexity of z-dimensional

(d) The C0 complexity of w dimensional

(e) The C0 complexity of u dimensional

(f) The C0 complexity of p-dimensional

(g) The C0 complexity of v-dimensional

FIGURE 9. **The C_0 complexity of each dimension.**

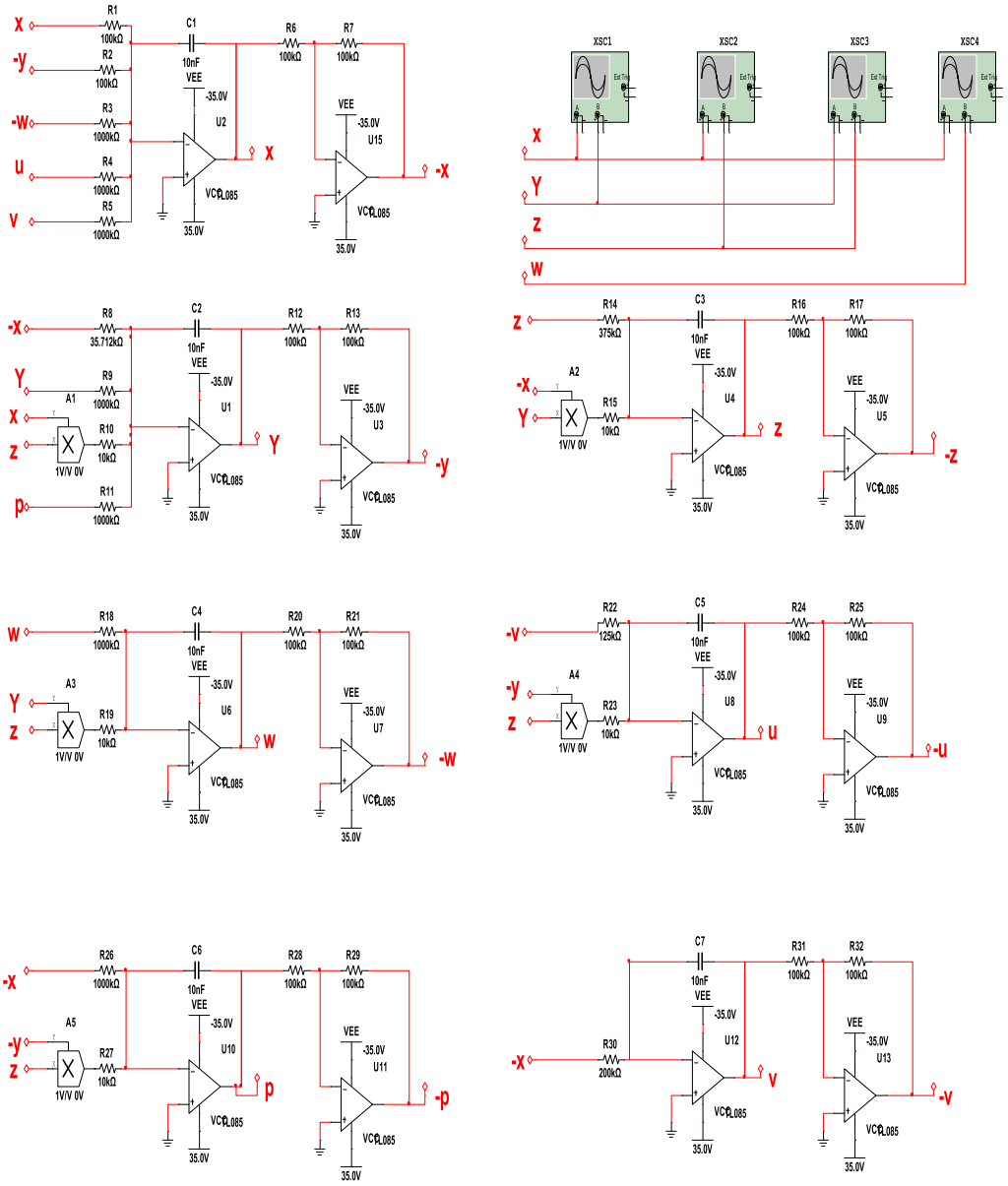

FIGURE 10. Circuit design for a new 7D hyperchaotic system.

is employed to implement information encryption in this paper.

In the state equation (12) of the drive system, x_d is selected as the drive variable.

$$\begin{cases} \dot{x_d} = a(y_d - x_d) + w_d - u_d - v_d \\ \dot{y_d} = cx_d - y_d - x_d z_d - p_d \\ \dot{z_d} = -bz_d + x_d y_d \\ \dot{w_d} = dw_d - y_d z_d \\ \dot{u_d} = ev_d + y_d z_d \\ \dot{p_d} = fx_d + y_d z_d \\ \dot{v_d} = rx_d \end{cases} \tag{12}$$

When the drive signal is x_d, the state equation of the synchronous system is:

$$\begin{cases} \dot{x_r} = a(y_r - x_d) + w_r - u_r - v_r \\ \dot{y_r} = cx_d - y_r - x_d z_r - p_r \\ \dot{z_r} = -bz_r + x_d y_r \\ \dot{w_r} = dw_r - y_r z_r \\ \dot{u_r} = ev_r + y_r z_r \\ \dot{p_r} = fx_d + y_r z_r \\ \dot{v_r} = rx_d \end{cases} \tag{13}$$

Comparing equations (12) with equation (13), it can be seen that the response system and the state equation of the drive system have the same form, but the chaotic signal x_r of

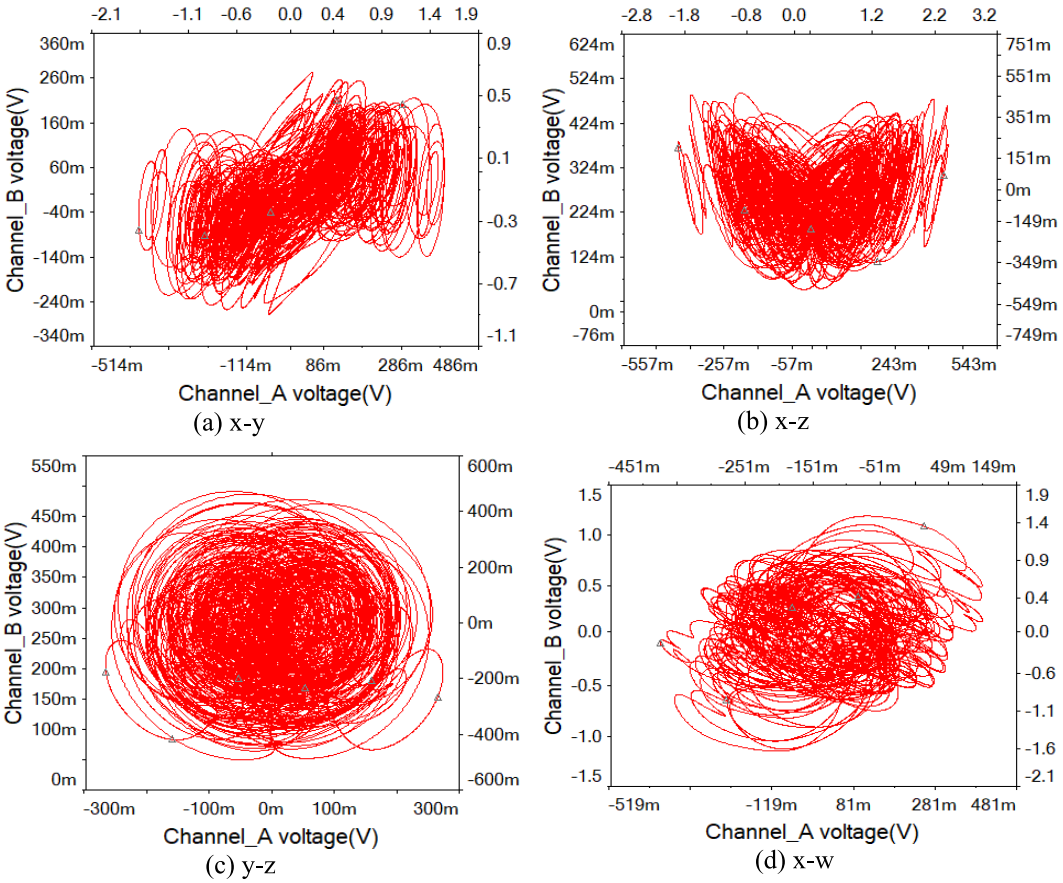

FIGURE 11. Chaotic system circuit simulation phase diagram: (a) x-y; (b) x-z; (c) y-z; (d) x-w.

the response system is replaced by the chaotic signal x_d in the drive system. When the drive system and the synchronization system are in an asynchronous state (At this time $a = 10$, $b = 8/3$, $c = 28$, $d = -1$, $e = 8$, $r = 3$, the initial condition of the drive system are $x = y = z = w = u = p = v = 1$, and the initial condition of the synchronization system are $x = 7, y = 0.01, z = 8, w = 19, u = 88, p = 7, v = 78$.), the errors between the drive system and the synchronization system are $e_x = x_d - x_r, e_y = y_d - y_r, e_z = z_d - z_r, e_w = w_d - w_r, e_u = u_d - u_r, e_p = p_d - p_r, e_v = v_d - v_r$. In Fig. 12, the variation of the errors $e_x, e_y, e_z, e_w, e_u, e_p, e_v$ with time can be clearly seen.

From the simulation results, even if the initial state of the drive system and the synchronous system is relatively large or even in a completely asynchronous state, the error is rapidly reduced to zero within 8 seconds by synchronous control. This shows that stable chaotic synchronization can be realized quickly, and the system can meet the requirements of secure communication.

B. CHAOTIC SYNCHRONIZATION SECURE COMMUNICATION CIRCUIT IMPLEMENTATION

Based on the drive response synchronization, the chaotic masking method to realize chaotic secret communication is used in this paper. The general diagram of a chaotic synchronous secure communication circuit is shown in Fig. 13. The detailed sub-circuit of a driving hierarchy block is basically identical to the circuit shown in Fig. 10 The difference is that the oscilloscope has been removed and two off-page connectors have been added to derive the X and Y signals to the main circuit. The encrypted signal is $S1 = -(Y(1) + S)$, where S is the signal generated by the square wave signal generator, and $Y(1)$ is the chaotic signal in the drive system. The decrypted signal is $S2$, $S2 = -(S1 + Y(2))$, where $Y(2)$ is the chaotic signal corresponding to $Y(1)$ in the response system.

In the preliminary test, the square wave was selected as the initial signal, and the initial values of the response system and the drive system were arbitrarily selected. The circuit simulation results are shown in Fig. 14, Fig. 15 and Fig. 16, when the input signal is $S = 0.1V$, the frequency is 8 Hz. Fig. 14 is a graph showing changes in a square wave signal with time. Fig. 15 is a graph showing the voltage signal variation over time after encryption, and Fig. 16 shows the voltage signal variation over time after decryption. To validate the comment that the original message is exactly recovered from the encrypted signal, the error between the original message and the decrypted message may is shown in Fig. 17.

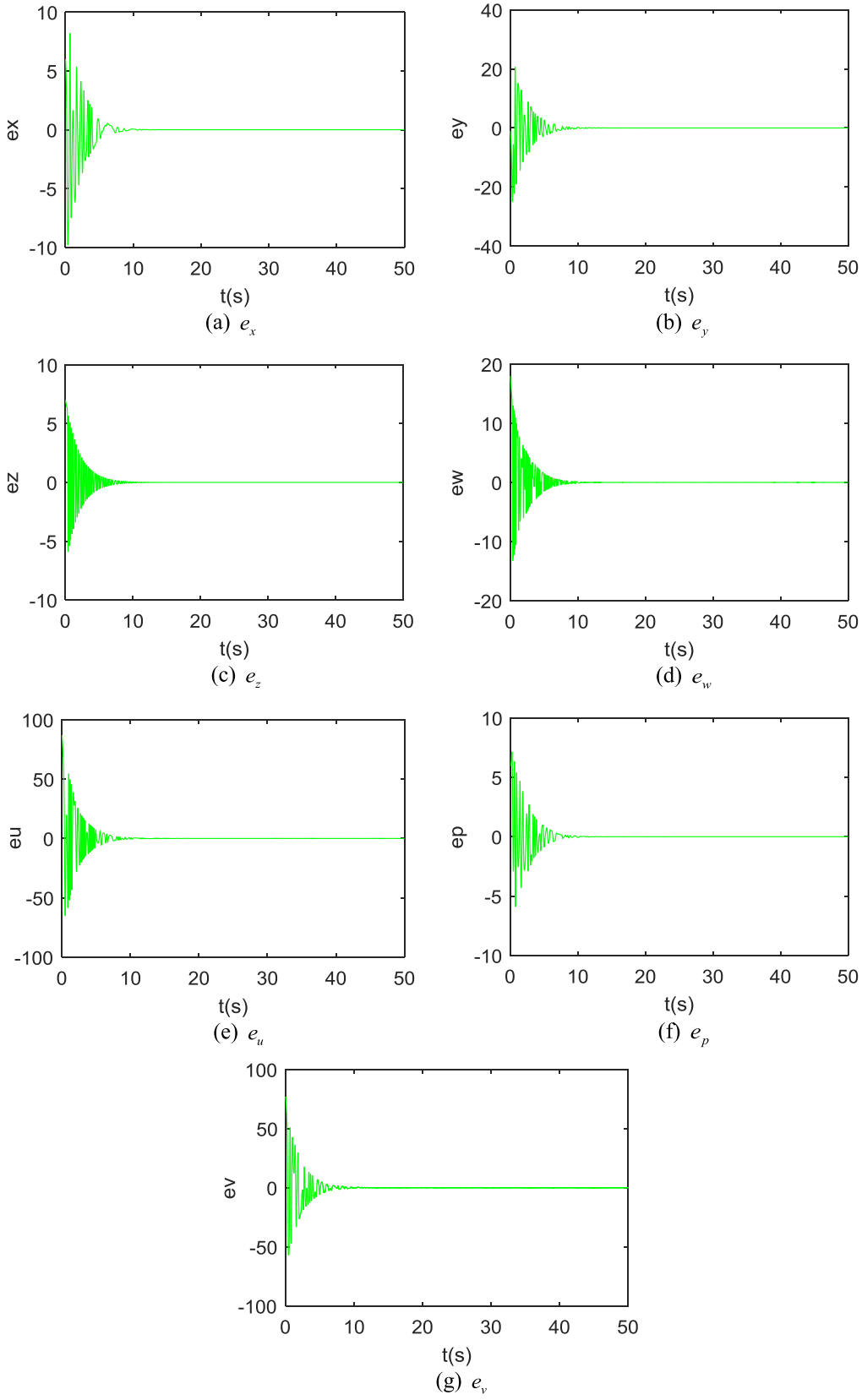

FIGURE 12. Error versus time graph.

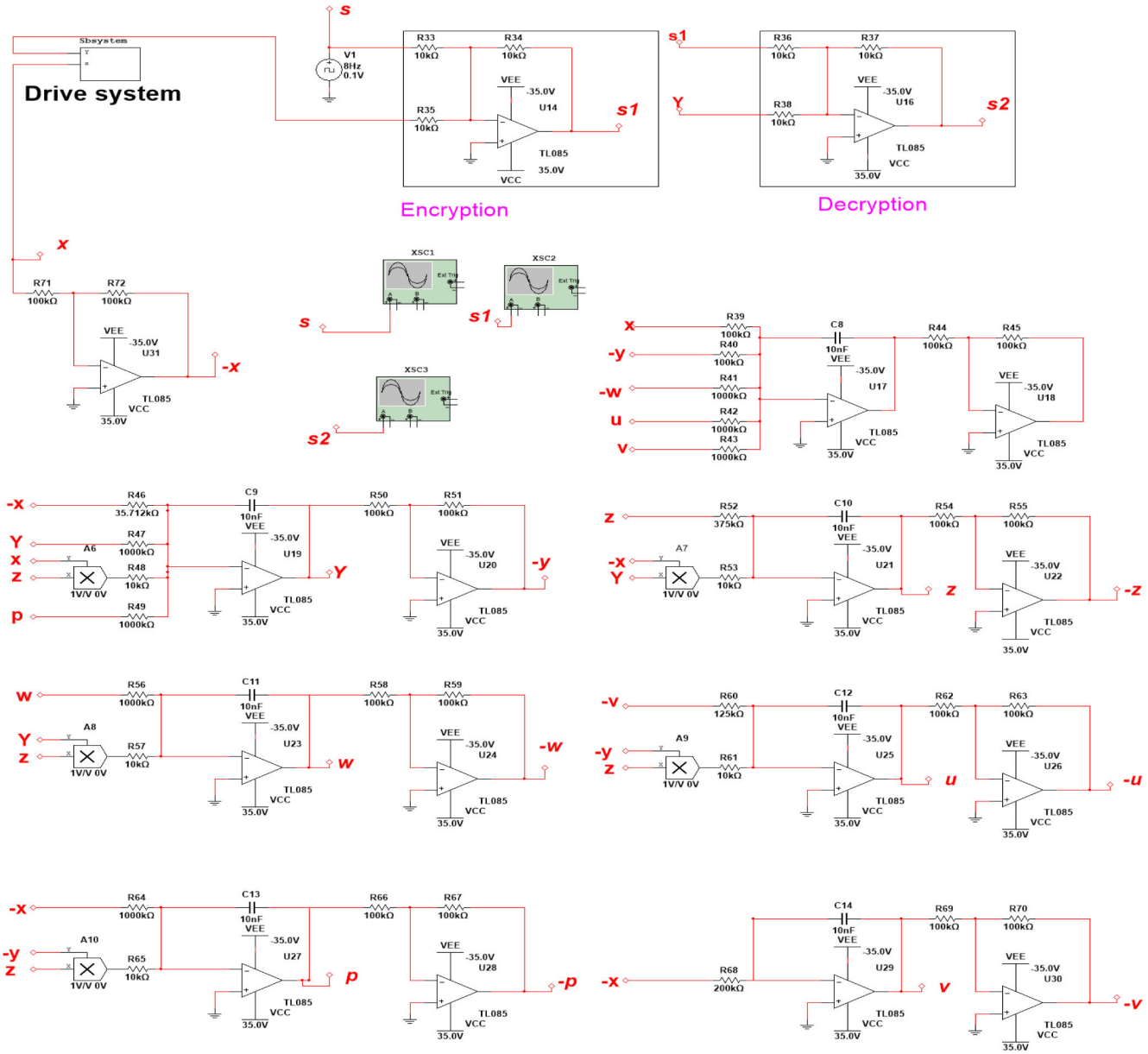

FIGURE 13. Chaotic synchronous secure communication circuit.

The physical diagram of the communication seven-dimensional hyperchaotic encryption and decryption circuit designed and implemented in this paper is shown in Fig. 18-19.

It can be seen from Figure 14-19 that when the system reaches chaotic synchronization, the original signal is basically consistent with the decrypted signal. It shows that the new chaotic circuit system can realize the encryption and decryption of the square wave voltage signal.

In order to verify the high adaptability of the secure communication of the hyperchaotic system proposed in this paper, the square wave signal S in the above circuit is replaced by a more complex signal $S5$, and the initial values of the drive system and the synchronization system are still arbitrarily selected.

The complex signal as the initial signal is superimposed by the sinusoidal signal $S3$ and the CHIRP signal $S4$. Due to its amplitude and frequency as a function of time, it is somewhat representative of some of the signals that actually exist. The maximum voltage value of the sinusoidal signal is 0.1V, and its frequency is 5Hz. The starting frequency of the CHIRP signal is 0.1 Hz, the final frequency is 60 Hz, the starting voltage is 0.1 V, the final voltage is 0.15 V, and the duration is 8 seconds.

The circuit diagram of the two signals superimposed is shown in Fig. 20. Fig. 21 is a graph showing changes in

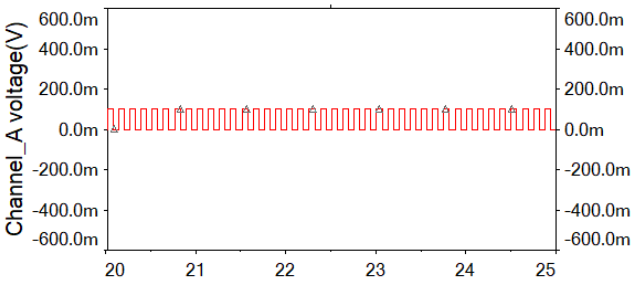

FIGURE 14. Voltage signal variation over time at the square wave signal generator.

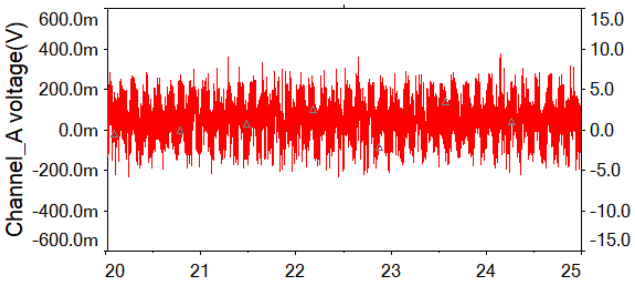

FIGURE 15. Voltage signal changing with time after encryption.

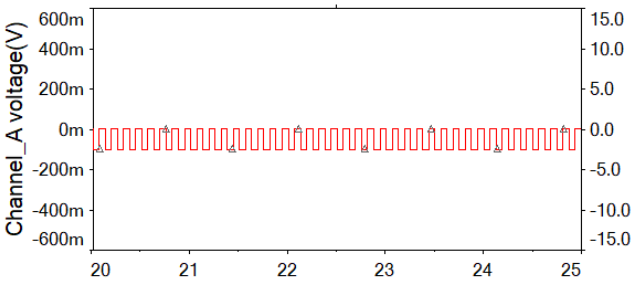

FIGURE 16. Voltage signal variation over time after decryption.

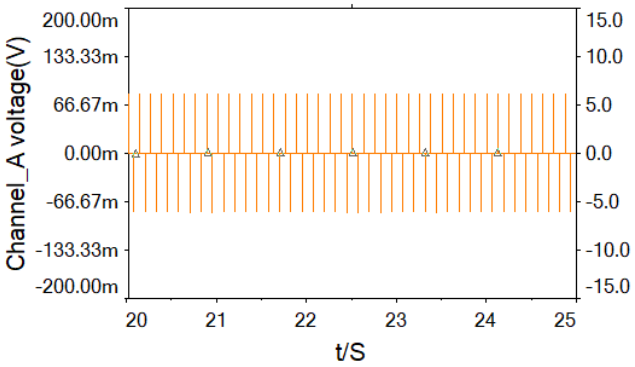

FIGURE 17. The error between the original message and the decrypted message.

voltage signals of complex signals over time. Fig. 22 is a graph showing changes in voltage signals over time after complex signal encryption, and Fig. 23 is a graph showing changes in voltage signals over time after decryption of complex signals. The error between the original message and the decrypted message may is shown in Fig. 24.

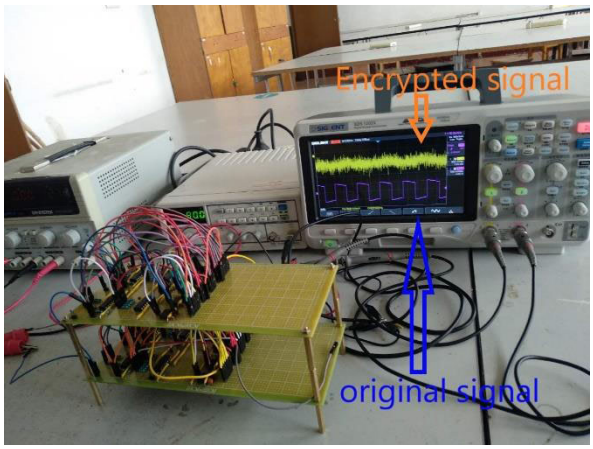

FIGURE 18. True encryption waveform.

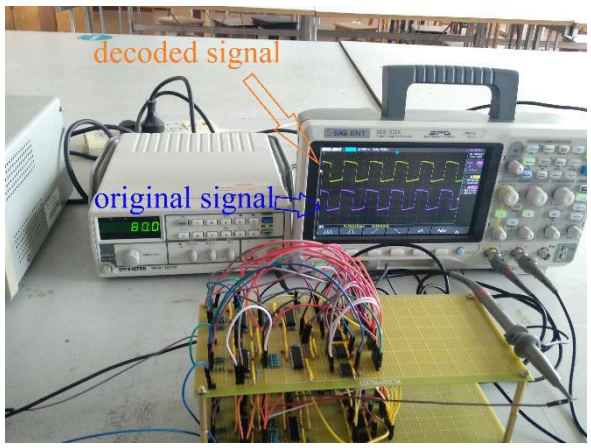

FIGURE 19. True decoded waveform.

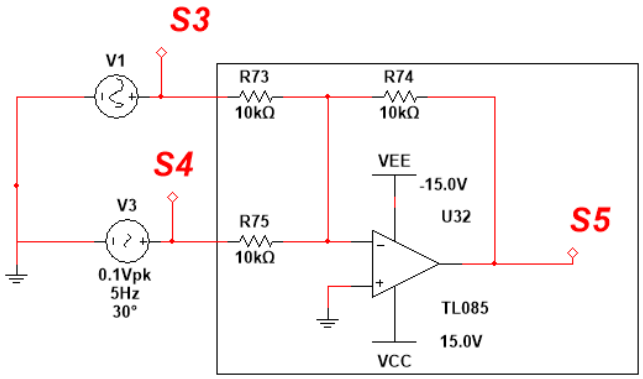

FIGURE 20. The circuit diagram of the two signals superimposed.

As shown in Fig. 20-22, when the system reaches chaotic synchronization, the comparison shows that the decrypted signal is basically the same as the original signal, indicating that the new chaotic circuit system also has encryption and decryption capabilities for more complex signals.

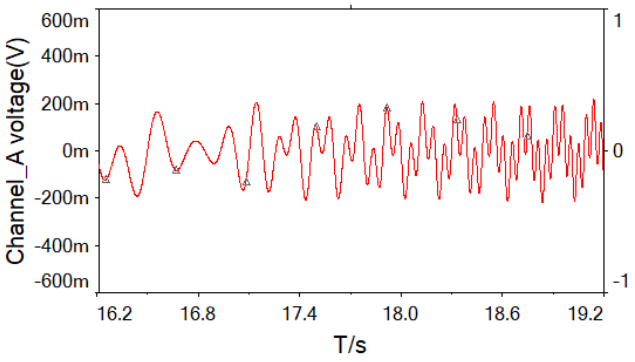

FIGURE 21. Voltage signals of complex signals over time.

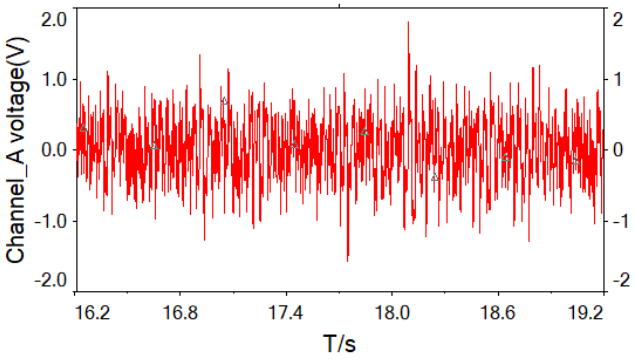

FIGURE 22. Voltage signals over time after complex signal encryption.

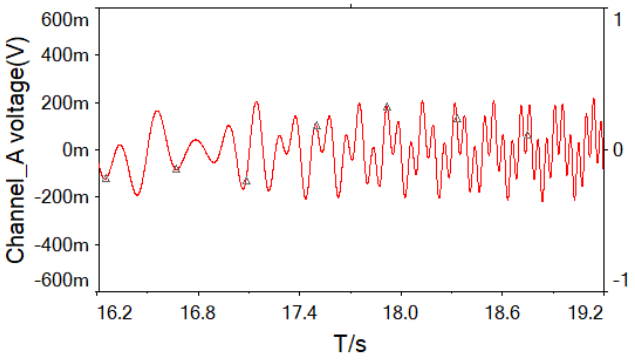

FIGURE 23. Voltage signals over time after decryption of complex signals.

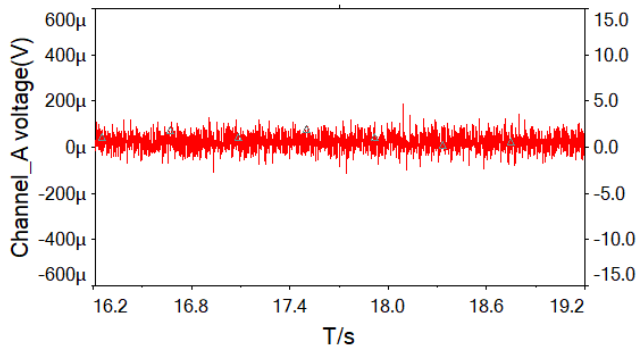

FIGURE 24. The error between the original message and the decrypted message.

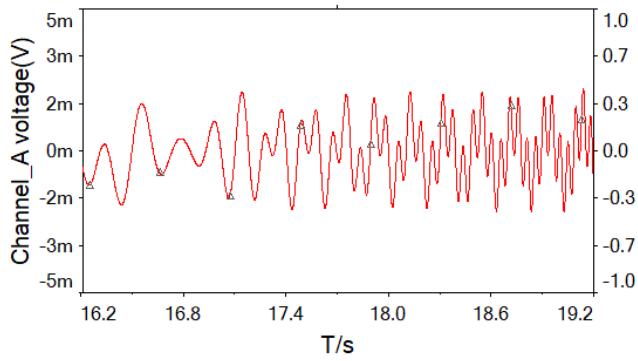

FIGURE 25. Complex signal voltage signal after processing changes with time.

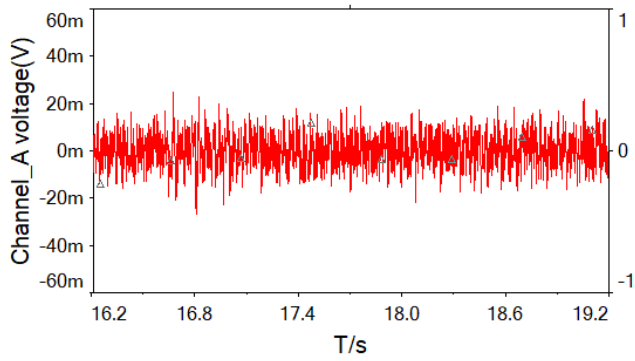

FIGURE 26. Decrypted voltage signal decrypted in an unauthorized manner.

In Fig. 24 we can see that there is still some error between the original signal and the decrypted signal. However, the original signal is 1000 times larger than the error signal, indicating that the original signal is consistent with the decrypted signal within the allowable range. Since this encryption and decryption circuit is almost the same as that proposed above, the encryption and decryption process of complex signals $S5$ is only realized by simulation.

C. SECURITY ANALYSIS

Take the encryption of the S5 signal as an example. Since the chaotic mask encryption method is adopted in this paper, the ratio of the voltage amplitude of the chaotic signal to the original signal affects the security performance of the secret circuit. Therefore, when encrypting, we can also use different resistance resistors in the addition circuit to reduce the original signal amplitude, which improves the security performance. Here, we change the resistance of resistor R34 from 10k to 0.1k. After the change, the voltage amplitude of the signal S5 is reduced by a factor of 100.

When unauthorized, the receiving end cannot know the specific resistance of the driving circuit, so the response circuit it has is inevitably difficult to be consistent with the

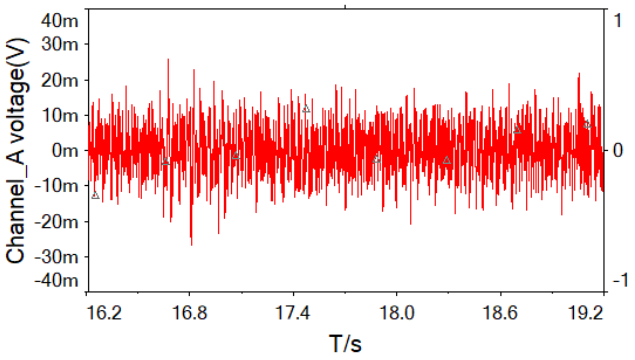

FIGURE 27. The error voltage signal of the original signal and the decrypted signal is decrypted in an unauthorized manner over time.

driving circuit, which may even have a huge gap. In the study, we found that the larger the difference between the resistance of the response circuit and the drive circuit, the lower the approximation of the signal waveform obtained after decryption and the original signal waveform. In this paper, in extreme conditions, only one resistor has a slight difference to perform circuit simulation.

When authorized, we can know the resistance of all resistors in the response circuit:

$$
\begin{aligned}
&R_{39} = 100\text{k}\Omega, \quad R_{40} = 100\text{k}\Omega, \; R_{41} = 1000\text{k}\Omega,\\
&R_{42} = 1000\text{k}\Omega, \quad R_{43} = 1000\text{k}\Omega, \; R_{44} = 100\text{k}\Omega,\\
&R_{45} = 100\text{k}\Omega, \quad R_{46} \approx 35.712\text{k}\Omega, \; R_{47} = 1000\text{k}\Omega,\\
&R_{48} = 10\text{k}\Omega, \quad R_{49} = 1000\text{k}\Omega, \; R_{50} = 100\text{k}\Omega,\\
&R_{51} = 100\text{k}\Omega, \quad R_{52} = 375\text{k}\Omega, \; R_{53} = 10\text{k}\Omega,\\
&R_{54} = 100\text{k}\Omega, \quad R_{17} = 100\text{k}\Omega, \; R_{18} = 1000\text{k}\Omega,\\
&R_{19} = 10\text{k}\Omega, \quad R_{20} = 100\text{k}\Omega, \; R_{21} = 100\text{k}\Omega,\\
&R_{22} = 125\text{k}\Omega, \quad R_{23} = 10\text{k}\Omega, \; R_{24} = 100\text{k}\Omega,\\
&R_{25} = 100\text{k}\Omega, \quad R_{26} = 1000\text{k}\Omega, \; R_{27} = 10\text{k}\Omega,\\
&R_{28} = 100\text{k}\Omega, \quad R_{29} = 100\text{k}\Omega. \; R_{30} = 200\text{k}\Omega,\\
&R_{31} = 100\text{k}\Omega, \quad R_{32} = 100\text{k}\Omega.
\end{aligned}
$$

When not authorized, it is assumed that under extreme conditions, only resistor R_{48} fails to impart the correct resistance, $R_{48} = 10.1k\Omega$, with a deviation of only 1%. The processed complex signal and the unauthorised decryption mode decrypted signal are respectively shown in Fig. 25 and 26, and the error voltages of both are shown in Fig. 27. In Fig. 27, the amplitude of the error voltage can be more than 20mV, and the amplitude of the complex signal voltage after processing is at most 2.5mV, which fully indicates that in this case, the decryption circuit of the unauthorized mode completely loses the decryption capability.

VI. CONCLUSION

This paper presents a novel seven-dimensional hyperchaotic system.

1.By designing a suitable controller, a seven-dimensional hyperchaotic system is obtained; The proposed hyperchaotic system has seven equations with only one equilibrium point.

2.The seven-dimensional hyperchaotic system has rich dynamic behavior including the equilibrium stability, dissipation, bifurcation and Lyapunov exponents. By adjusting the linear control parameters, various dynamic behaviors occur, and the shortcomings of the hyperchaotic parameter range can be eliminated.

3. The numerical simulation is consistent with the circuit simulation results, and the obtained phase image is the same as the experimental simulation results. The results verify the correctness and effectiveness of the proposed seven-dimensional hyperchaotic system and indicate the correctness and physical achievability of the seven-dimensional hyperchaotic system design.

4.The chaotic secure communication circuit is composed of 7D chaotic circuit with optimized design, and the secure communication is realized by analog electronic circuit. The experimental results prove the effectiveness of the designed scheme.

REFERENCES

[1] Z. Wei, P. Yu, W. Zhang, and M. Yao, "Study of hidden attractors, multiple limit cycles from Hopf bifurcation and boundedness of motion in the generalized hyperchaotic Rabinovich system," *Nonlinear Dyn.*, vol. 82, nos. 1–2, pp. 131–141, 2015.

[2] A. Akgul, S. Hussain, and I. Pehlivan, "A new three-dimensional chaotic system, its dynamical analysis and electronic circuit applications," *Optik*, vol. 127, no. 18, pp. 7062–7071, 2016.

[3] Z. Wei, V.-T. Pham, T. Kapitaniak, and Z. Wang, "Bifurcation analysis and circuit realization for multiple-delayed Wang–Chen system with hidden chaotic attractors," *Nonlinear Dyn.*, vol. 85, no. 3, pp. 1635–1650, 2016.

[4] J. P. Singh and B. K. Roy, "Crisis and inverse crisis route to chaos in a new 3-D chaotic system with saddle, saddle foci and stable node foci nature of equilibria," *Optik*, vol. 127, no. 24, pp. 11982–12002, 2016.

[5] S. M. T. Nezhad, M. Nazari, and E. A. Gharavol, "A novel DoS and DDoS attacks detection algorithm using ARIMA time series model and chaotic system in computer networks," *IEEE Commun. Lett.*, vol. 20, no. 4, pp. 700–703, Apr. 2016.

[6] Z. Wei, I. Moroz, J. C. Sprott, Z. Wang, and W. Zhang, "Detecting hidden chaotic regions and complex dynamics in the self-exciting homopolar disc dynamo," *Int. J. Bifurcation Chaos*, vol. 27, no. 2, 2017, Art. no. 1730008.

[7] J. P. Singh and B. K. Roy, "The simplest 4-D chaotic system with line of equilibria, chaotic 2-torus and 3-torus behaviour," *Nonlinear Dyn.*, vol. 89, no. 3, pp. 1845–1862, 2017.

[8] Z. Wang, A. Akgul, V.-T. Pham, and S. Jafari, "Chaos-based application of a novel no-equilibrium chaotic system with coexisting attractors," *Nonlinear Dyn.*, vol. 89, no. 3, pp. 1877–1887, 2017.

[9] J. P. Singh and B. K. Roy, "Second order adaptive time varying sliding mode control for synchronization of hidden chaotic orbits in a new uncertain 4-D conservative chaotic system," *Trans. Inst. Meas. Control*, vol. 40, no. 13, pp. 3573–3586, 2017.

[10] C. Li, J. C. Sprott, W. Hu, and Y. Xu, "Infinite multistability in a self-reproducing chaotic system," *Int. J. Bifurcation Chaos*, vol. 27, no. 10, 2017, Art. no. 1750160.

[11] J. P. Singh, K. Lochan, N. V. Kuznetsov, and B. K. Roy, "Coexistence of single- and multi-scroll chaotic orbits in a single-link flexible joint robot manipulator with stable spiral and index-4 spiral repellor types of equilibria," *Nonlinear Dyn.*, vol. 90, no. 2, pp. 1277–1299, 2017.

[12] Z. Wei, I. Moroz, J. C. Sprott, A. Akgul, and W. Zhang, "Hidden hyperchaos and electronic circuit application in a 5D self-exciting homopolar disc dynamo," *Chaos*, vol. 27, no. 3, 2017, Art. no. 033101.

[13] V. R. F. Signing and J. Kengne, "Coexistence of hidden attractors, 2-torus and 3-torus in a new simple 4-D chaotic system with hyperbolic cosine nonlinearity," *Int. J. Dyn. Control*, vol. 6, no. 4, pp. 1421–1428, 2018.

[14] S. Vaidyanathan, A. Sambas, S. Kacar, and Ü. Çavuşoğlu, "A new three-dimensional chaotic system with a cloud-shaped curve of equilibrium points, its circuit implementation and sound encryption," *Int. J. Model., Identificat. Control*, vol. 30, no. 3, pp. 184–196, 2018.

[15] Z. Wei, V.-T. Pham, A. J. M. Khalaf, J. Kengne, and S. Jafari, "A modified multistable chaotic oscillator," *Int. J. Bifurcation Chaos*, vol. 28, no. 7, 2018, Art. no. 1850085.

[16] N. Smaoui, A. Karouma, and M. Zribi, "Secure communications based on the synchronization of the hyperchaotic Chen and the unified chaotic systems," *Commun. Nonlinear Sci. Numer. Simul.*, vol. 16, no. 8, pp. 3279–3293, 2011.

[17] B. Wang and X. Dong, "Secure communication based on a hyperchaotic system with disturbances," *Math. Problems Eng.*, vol. 2015, Sep. 2014, Art. no. 616137.

[18] J. Lü and G. Chen, "A new chaotic attractor coined," *Int. J. Bifurcation Chaos*, vol. 12, no. 3, pp. 659–661, 2002.

[19] C.-L. Li, J.-B. Xiong, and W. Li, "A new hyperchaotic system and its generalized synchronization," *Optik*, vol. 125, no. 1, pp. 575–579, 2014.

[20] G. Qi, G. Chen, S. Du, Z. Chen, and Z. Yuan, "Analysis of a new chaotic system," *Phys. A, Stat. Mech. Appl.*, vol. 352, pp. 295–308, Jul. 2005.

[21] J. H. Lu and G. R. Chen, "Generating multiscroll chaotic attractors: Theories, methods and applications," *Int. J. Bifurcation Chaos*, vol. 16, no. 4, pp. 775–858, 2016.

[22] O. E. Rössler, "An mech equation for hyperchaos," *Phys. Lett. A*, vol. 71, nos. 2–3, pp. 155–157, 1979.

[23] J. P. Singh and B. K. Roy, "The nature of Lyapunov exponents is $(+, +, -, -)$. Is it a hyperchaotic system?" *Chaos, Solitons & Fractals*, vol. 92, pp. 73–85, Nov. 2016.

[24] S. Vaidyanathan, A. T. Azar, K. Rajagopal, A. Sambas, S. Kacar, and U. Cavusoglu, "A new hyperchaotic temperature fluctuations model, its circuit simulation, FPGA implementation and an application to image encryption," *Int. J. Simul. Process Model.*, vol. 13, no. 3, pp. 281–296, 2018.

[25] J. P. Singh and B. K. Roy, "Hidden attractors in a new complex generalised lorenz hyperchaotic system, its synchronisation using adaptive contraction theory, circuit validation and application," *Nonlinear Dyn.*, vol. 92, no. 2, pp. 373–394, 2018.

[26] T. Yang, L.-B. Yang, and C.-M. Yang, "Cryptanalyzing chaotic secure communications using return maps," *Phys. Lett. A*, vol. 245, no. 6, pp. 495–510, 1998.

[27] Z. Li, K. Li, C. Wen, and Y. C. Soh, "A new chaotic secure communication system," *IEEE Trans. Commun.*, vol. 51, no. 8, pp. 1306–1312, Aug. 2003.

[28] G. Álvarez, F. Montoya, M. Romera, and G. Pastor, "Breaking parameter modulated chaotic secure communication system," *Chaos Solitons Fractals*, vol. 21, no. 4, pp. 783–787, 2004.

[29] S. Behnia, A. Akhshani, H. Mahmodi, and A. Akhavan, "A novel algorithm for image encryption based on mixture of chaotic maps," *Chaos, Solitons, Fractals*, vol. 35, no. 2, pp. 408–419, 2008.

[30] A. Bogris, A. Argyris, and D. Syvridis, "Encryption efficiency analysis of chaotic communication systems based on photonic integrated chaotic circuits," *IEEE J. Quantum Electron.*, vol. 46, no. 10, pp. 1421–1429, Oct. 2010.

[31] R. M. Nguimdo, P. Colet, L. Larger, and L. Pesquera, "Digital key for chaos communication performing time delay concealment," *Phys. Rev. Lett.*, vol. 107, no. 3, 2011, Art. no. 034103

[32] J. Pan, Q. Ding, and B. Du, "A new improved scheme of chaotic masking secure communication based on lorenz system," *Int. J. Bifurcation Chaos*, vol. 22, no. 5, pp. 147–505, 2012.

[33] L.-Z. Liu, J. Zhang, G.-X. Xu, L.-S. Liang, and M.-S. Wang, "A chaotic secure communication method based on chaos systems partial series parameter estimation," *Acta Phys. Sinica*, vol. 63, no. 1, pp. 247–254, 2014.

[34] B. Nana and P. Woafo, "Chaotic masking of communication in an emitter–relay–receiver electronic setup," *Nonlinear Dyn.*, vol. 82, nos. 1–2, pp. 899–908, 2015.

[35] Q. Wang, S. Yu, C. Li, J. Lü, X. Fang, C. Guyeux, and J. M. Bahi, "Theoretical design and FPGA-based implementation of higher-dimensional digital chaotic systems," *IEEE Trans. Circuits Syst. I, Reg. Papers*, vol. 63, no. 3, pp. 401–412, Mar. 2016.

[36] M. F. Hassan, "Synchronization of uncertain constrained hyperchaotic systems and chaos-based secure communications via a novel decomposed nonlinear stochastic estimator," *Nonlinear Dyn.*, vol. 83, no. 4, pp. 2183–2211, 2016.

[37] J. Oden, R. Lavrov, Y. K. Chembo, and L. Larger, "Multi-Gbit/s optical phase chaos communications using a time-delayed optoelectronic oscillator with a three-wave interferometer nonlinearity," *Chaos*, vol. 27, no. 11, 2017, Art. no. 114311.

[38] S. Chen, S. Yu, J. Lü, G. Chen, and J. He, "Design and FPGA-based realization of a chaotic secure video communication system," *IEEE Trans. Circuits Syst. Video Technol.*, vol. 28, no. 9, pp. 2359–2371, Sep. 2018.

[39] H. Natiq, S. Banerjee, M. R. K. Ariffin, and M. R. M. Said, "Can hyperchaotic maps with high complexity produce multistability?" *Chaos*, vol. 29, Jan. 2019, Art. no. 011103. doi: 10.1063/1.5079886.

[40] J. C. Sprott, "A proposed standard for the publication of new chaotic systems," *Int. J. Bifurcation Chaos*, vol. 21, no. 9, pp. 2391–2394, 2011.

[41] J. Wang, W. Yu, J. Wang, Y. Zhao, J. Zhang, and D. Jiang, "A new six-dimensional hyperchaotic system and its secure communication circuit implementation," *Int. J. Circuit Theory Appl.*, vol. 47, no. 5, pp. 702–717, 2019. doi: 10.1002/cta.2617.

[42] H. Liu, H. Wan, C. K. Tse, and J. Lü, "An encryption scheme based on synchronization of two-layered complex dynamical networks," *IEEE Trans. Circuits Syst. I, Reg. Papers*, vol. 63, no. 11, pp. 2010–2021, Nov. 2016.

[43] S. Vaidyanathan, A. Sambas, M. Mamat, and M. Sanjaya, "Analysis, synchronisation and circuit implementation of a novel jerk chaotic system and its application for voice encryption," *Int. J. Model., Identificat. Control*, vol. 28, no. 2, pp. 153–166, 2017.

[44] C. Li, D. Lin, B. Feng, J. Lü, and F. Hao, "Cryptanalysis of a chaotic image encryption algorithm based on information entropy," *IEEE Access*, vol. 6, pp. 75834–75842, 2018.

WENXIN YU received the B.Sc. degree in applied mathematics from Hebei Normal University, Shijiazhuang, China, in 2005, the M.S. degree in wavelet analysis from the Changsha University of Science and Technology, Changsha, in 2008, and the Ph.D. degree in electrical engineering from Hunan University, Changsha, in 2015. He joined the Hunan University of Science and Technology, where he is currently a Lecturer with the School of Information and Electrical Engineering. His research interests include intelligent control, fault diagnosis, signal processing, wavelet analysis, and its application.

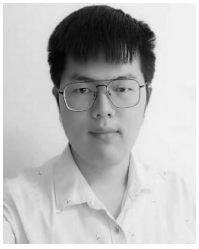

JING WANG is currently pursuing the B.E. degree with the Hunan University of Science and Technology. His research interest includes circuit design and control.

JUNNIAN WANG received the B.Sc. degree in physics and the M.S. degree in radio physics from Lanzhou University, Lanzhou, China, in 1991 and 2000, respectively, and the Ph.D. degree in control theory and control engineering from Central South University, Changsha, in 2006. He joined the Hunan University of Science and Technology, where he is currently a Professor with the School of Physics and Electronics. His research interests include complex systems, intelligent control, and intelligent fault diagnosis.

HONGPING ZHU is currently a Professor with the School of Information and Electrical Engineering, Hunan University of Science and Technology. Her research interests include high voltage technology and intelligent detection and control.

MU LI received the B.Sc. degree in electronic technology from Hunan Normal University, Changsha, China, in 2002, and the M.Sc. and Ph.D. degrees in circuit and system from Hunan University, Changsha, in 2007 and 2014, respectively. He is currently an Associate Professor with Hunan University of Science and Technology. His research interests include intelligent signal processing, switched current technology, analog filter design, fractional order system and testing, and fault diagnosis of analog and mixed-signal circuits.

YAN LI is currently a Lecturer with the School of Information and Electrical Engineering, Hunan University of Science and Technology. Her research interests include signal processing, intelligent control, and fault diagnosis.

DAN JIANG received the B.E. degree in electrical engineering from the Hunan University of Science and Technology, Xiangtan, in 2016, where she is currently pursuing the M.S. degree. Her research interests include intelligent algorithm and faults diagnostic analysis.